JOURNAL OF PETROLOGY | VOLUME 40 | NUMBER 2 | PAGES 339–362 | 1999

Some Phase Equilibrium Constraints on the Origin of Proterozoic (Massif) Anorthosites and Related Rocks

JOHN LONGHI[1]*, JACQUELINE VANDER AUWERA[2], MIRANDA S. FRAM[3] AND JEAN-CLAIR DUCHESNE[2]

[1]LAMONT–DOHERTY EARTH OBSERVATORY, RT. 9W, PALISADES, NY 10964, USA

[2]L.A. GÉOLOGIE, PÉTROLOGIE, GÉOCHIMIE, UNIVERSITÉ DE LIÈGE, 4000 LIÈGE, BELGIUM

[3]DEPARTMENT OF GEOLOGY, UNIVERSITY OF CALIFORNIA, DAVIS, CA 95616, USA

RECEIVED MAY 20, 1997; REVISED TYPESCRIPT ACCEPTED JUNE 26, 1998

Experimental data in the range of 1 bar to 13 kbar enable us to map the liquidus equilibria relevant to Proterozoic (massif) anorthosites and related mafic rocks. Massif anorthosites are widely believed to have formed by accumulation of plagioclase into high-Al basaltic liquids. Mantle-derived basaltic liquids, fractionating at pressures sufficiently high (10–13 kbar) to crystallize the highly aluminous orthopyroxene megacrysts typically observed in anorthosite massifs, reach plagioclase saturation at low normative silica contents. Peritectic-like equilibria (e.g. liq + opx → plag + cpx + sp) and a thermal divide on the plagioclase + pyroxene liquidus surface ensure that mantle-derived liquids become nepheline normative with further crystallization and crustal assimilation at depth. Such liquids cannot produce the full range of troctolitic–noritic to troctolitic–gabbroic mineral assemblages observed in anorthosite massifs without extensive low-pressure granite assimilation. Conversely, the array of plausible anorthosite parental liquids not only lies along the trace of the plagioclase + two-pyroxene cotectic from 10 to 13 kbar, but also straddles the thermal divide on the plagioclase + pyroxene liquidus surface. This condition requires mafic source regions, such as lower continental crust or foundered mafic plutons, for liquids parental to massif anorthosites and associated mafic intrusions.

KEY WORDS: *anorthosite; lower crust; megacryst; thermal divide; troctolite*

INTRODUCTION

There is hardly a consensus on the petrogenesis of Proterozoic (massif) anorthosites, but many investigators believe in a petrogenetic scheme that involves at least two major stages: (1) extensive crystallization (± assimilation) of a mantle-derived magma ponded at or near the base of the crust that produces suspensions of plagioclase in Fe-rich, high-Al gabbroic liquids; followed by (2) intrusion of these suspensions into the mid–upper crust where they form complex magma chambers (e.g. Duchesne, 1984; Emslie, 1985; Ashwal, 1993; Wiebe, 1994). A key component of the scheme is the presence in most massifs of high-Al orthopyroxene megacrysts (HAOM, Emslie, 1975) that appear to preserve a record of the high-pressure stage (Maquil & Duchesne, 1984; Longhi *et al.*, 1993). The structures of massifs vary from those that are composites of multiple diapiric intrusions (Harp Lake, Emslie, 1980; Rogaland, Duchesne, 1984) to intrusive bodies with well-developed layering of leucocratic troctolites and leuconorites or leucogabbros overlain by masses of anorthosite (Michikamau, Emslie, 1970; Laramie, Frost *et al.*, 1993), so there may be different modes of transport of the suspensions through the crust. Associated mafic rocks are found on all scales from large layered intrusions, such as Kiglapait (Morse, 1979) and Bjerkreim–Sokndal (Duchesne, 1987; Wilson *et al.*, 1996), with dimensions on the same scale as the anorthositic bodies, to lenses, dikes, and small ferrodioritic

*Corresponding author.

(jotunitic) to monzonitic (mangeritic) intrusions that appear to have formed from liquids residual to either the crystallization of the anorthositic masses (e.g. Mitchell *et al.*, 1996) or the more primitive mafic intrusion (e.g. Vander Auwera *et al.*, 1998). Many workers believe the parental magmas of the large layered intrusions to have been relatively plagioclase-free residual liquid from the deep-seated chambers (e.g. Wiebe, 1994). Finally, most workers ascribe formation of associated granitoids (quartz monzonite, charnockite) to melting of the lower crust (e.g. Emslie *et al.*, 1994), although some examples of continuous differentiation from jotunite to charnockite exist (Vander Auwera *et al.*, 1998).

The major alternative to derivation of the anorthosites' parental magma from the mantle is melting of the lower crust. Trace element modelling provides the basis for this hypothesis (Simmons & Hanson, 1978; Taylor *et al.*, 1984), although there is some experimental work to support melting of the lower crust as well (Green, 1969).

Most anorthositic and related rocks have isotopic compositions that depart to some degree from depleted mantle evolution curves in the direction of crustal contamination—usually the mafic rocks are more contaminated—leading to the concept that most mafic rocks are 'coeval, but not consanguineous' with the anorthosites (e.g. Duchesne *et al.*, 1989). Where massifs lie on either side of a major tectonic boundary, there are systematic differences in the isotopic compositions that correlate with tectonic province (Ashwal & Wooden, 1983; Emslie *et al.*, 1994). Assimilation of different crustal types in the ponded, deep-seated chamber and possibly additional assimilation during transit of the magmas to the upper crust are believed to account for departures of the isotopic systems from mantle evolution curves (e.g. Emslie *et al.*, 1994).

The purpose of this paper is to examine the viability of evolved mantle-derived magmas as parental magmas not only to the anorthositic rocks, but to the mafic rocks and high-Al orthopyroxene megacrysts. To this end we have employed new and published experimental phase equilibrium data in the range of 1 bar to 13 kbar to map out permissible liquid lines of descent of mantle-derived magmas, to constrain the compositions of liquids parental to massif anorthosites based on crystallization sequences, and to predict the compositions of possible lower-crustal melts under anhydrous conditions. We have distinguished two groups of compositions for consideration on the basis of *mg*-number [molar MgO/(MgO + FeO)] and the composition of the normative feldspar: a high-Al basaltic group (*mg*-number = 0·5–0·4; $Ab_{42–50}Or_{4–8}$) represented by HLCA, the proposed parent magma of the Harp Lake complex (Emslie, 1980), and a jotunitic group (*mg*-number = 0·4–0·25; $Ab_{51–66}Or_{9–20}$) represented by TJ, a chill margin sample from the Bjerkreim–Sokndal intrusion of southern Norway (Duchesne & Hertogen, 1988). Although the liquidus temperatures of the jotunites are much lower than those of the HLCA group, their phase relations are broadly similar, and it is likely that the groupings represent distinct portions of a larger continuum of compositions.

EXPERIMENTAL METHODS

New experiments were carried out on a powdered rock from the Hettasch Intrusion in Nain, Labrador (Berg, 1980) and on a series of synthetic crystal–glass mixtures. The Hettasch sample (HT76E) is one of a series of samples from quenched pillow-like masses within the layered cumulates. Interpretations of these rocks range from chilled pulses of new liquid (Berg, 1980) to negatively buoyant mixtures of crystals and liquid detached from the top of the magma chamber. The synthetic materials include HLCA, the average high-Al gabbro and proposed parental magma composition of the Harp Lake anorthosite in Nain, Labrador (Emslie, 1980), and HLOL, a composition designed to yield olivine-bearing multisaturated liquids at moderate pressures. A mechanical mixture of HLCA and HT76E was also used as starting material. The synthetic materials were fused mixtures of oxides and carbonates that were partially crystallized at the fayalite–magnetite–quartz (FMQ) buffer. All experiments were performed at Lamont–Doherty Earth Observatory in a standard 1/2 inch piston cylinder apparatus, utilizing a $BaCO_3$ pressure medium, and calibrating pressure against the melting curve of gold, as described by Fram & Longhi (1992). Temperature was measured with Pt_{100}–$Pt_{90}Rh_{10}$ thermocouples and power consumption was monitored to guard against thermocouple drift. Charges were run in unsealed graphite capsules. Comparison of oxide assemblages produced in graphite capsules at 5 kbar with 1 atm controlled fO_2 experiments indicates that fO_2 is approximately at MW (magnetite–wüstite) − 2 in the graphite capsule experiments (Vander Auwera & Longhi, 1994). Also, IR spectra of glass produced with the same assembly indicated $\leq 0{\cdot}1\%$ each of H_2O and CO_2 (Fram & Longhi, 1992). Bulk compositions of the starting materials are listed in Table 1. Run conditions and phase assemblages are given in Table 2.

After each experiment, the charges were mounted in epoxy, polished and analyzed with the CAMEBAX electron microprobe utilizing the wavelength dispersive system. Accelerating voltage was set at 15 kV and all elements were measured for 20 s at a beam current of 25 nA except in the case of feldspars, phosphates, and glasses, when Na and K were measured first for 30 s at 5–10 nA. For glasses the beam was rastered over square areas 10–20 μm on a side to minimize alkali loss. X-ray intensities were reduced using the Cameca PAP

Table 1: Analyzed and nominal compositions of starting materials and parent magmas (wt % oxides)

	HLOL*†	HT80E*‡	HLCA*†	HT/HL§	TJ*‡	KIMOD¶
SiO_2	46·9	46·9	50·0	48·9	49·5	49·1
TiO_2	1·78	1·10	1·85	1·49	3·46	0·79
Al_2O_3	16·7	19·6	17·5	18·7	16·0	18·7
Cr_2O_3	0·03	0·02	0·03	0·02	0·00	
FeO	12·2	10·8	10·8	10·9	13·1	10·3
MgO	10·5	7·75	6·67	7·29	4·54	7·78
MnO	0·13	0·15	0·15	0·15	0·13	0·15
CaO	8·49	8·78	8·78	8·86	6·82	9·52
K_2O	0·47	0·40	0·44	0·42	0·94	0·27
Na_2O	2·85	2·82	2·93	2·90	3·65	3·08
P_2O_5	0·18	0·15	0·16	0·16	0·63	0·11
Sum	100·2	98·5	99·5	99·8	98·8	99·8
mg-no.	0·607	0·539	0·520	0·544	0·383	0·574
NAb	0·428	0·391	0·423	0·399	0·506	0·409
NOr	0·046	0·034	0·042	0·038	0·089	0·065

mg-number = molar MgO/(MgO + FeO).
NAb = $2Na_2O/(Al_2O_3 + Na_2O + K_2O)$;
NOr = $2K_2O/(Al_2O_3 + Na_2O + K_2O)$.
* Analyzed compositions.
† Devitrified synthetic glass.
‡ Rock powder.
§ A 50:50 mixture of normalized HT80E and HLCA.
¶ Model Kiglapait parent magma from Nolan & Morse (1986).

correction program. A combination of mineral and glass standards were used for glass analyses, whereas only mineral standards were used for plagioclase, Fe–Ti oxides, pyroxenes, and olivines. Major element compositions of the experimental phases are reported in Table 3.

Mass balance between the bulk composition of the starting material and the compositions of all phases present in each run has been calculated using a least-squares multiple regression to determine phase proportions and to evaluate the approach to bulk equilibrium. Results are given in Table 2. In each case residual sums of the squares are acceptably low, but in some runs the regression yields negative amounts of low-Ca pyroxene. In the case of the runs with powdered rock starting materials (HT80E-1 and -5) the negative values for orthopyroxene are the result of the regression compensating for non-negligible proportions of relict olivine (armored by clinopyroxene) that is not included in the regression. In the case of run HLCA-53 the negative value for pigeonite (–0·016) is probably the result of incomplete re-equilibration of the high-pressure phases grown in the first stage of this experiment (note the relatively high RSSQ in Table 2). In the case of run HLOL-3 the slightly negative proportion of orthopyroxene (–0·0079) is probably a combination of a small analytical error and a reaction between orthopyroxene and liquid to form low-Ca clinopyroxene gone nearly to completion. Although the presence of relict olivine and calculated negative proportions of low-Ca pyroxene reflect incomplete bulk equilibration, it is very likely that these runs closely approached equilibrium

Table 2: Experiments and run conditions

Run	*T* (°C)	*P* (kbar)	Time (h)	Run products	Phase proportions*	RSSQ	$K_D^{opx-liq}$
HT80E-1	1265	11·5	51·5	gl, cpx, plag, sp, opx, [ol]	0·697, 0·225, 0·053, 0·042 –0·018†	0·03	0·281
HT80E-4	1300	13	53·5	gl, gar, cpx, plag, [ol]	0·744, 0·193, 0·046, 0·013	0·10	
HT80E-5	1265	10	49·0	gl, pig, plag, aug, sp, opx, [ol]	0·676, 0·240, 0·122, 0·055, 0·039, –0·135†	0·02	0·264
HT80E-6	1350/1265	13	2/92·5	gl, gar, cpx, plag	0·344, 0·342, 0·205, 0·110	0·20	
HT80E-7	1275	10	24·0	gl, opx, plag, sp	0·883, 0·047, 0·044, 0·025	0·05	0·279
HT/HL-1	1270	11·5	44·7	gl, plag, opx, cpx	0·628, 0·187, 0·094, 0·089	0·08	0·280
HLCA-25	1250	13	34·0	gl, plag, cpx, opx	0·674, 0·154, 0·136, 0·029	0·11	0·297
HLCA-44	1175	6	48·0	gl, plag, pig	0·326, 0·433, 0·232	0·14	
HLCA-53	1270/1200	11·5/6	72/116	gl, plag, opx, ol, pig	0·725, 0·194, 0·097, 0·007, –0·016	0·37	0·259
HLCA-55	1200/1260	6/11·5	67/119	gl, plag, cpx, opx	0·756, 0·118, 0·082, 0·046	0·11	0·279
HLOL-3	1265	11·5	49·0	gl, cpx, sp, opx	0·573, 0·402, 0·039, –0·007	0·55	0·249
HLOL-4	1300	11·5	29·5	gl, cpx, opx, sp	0·807, 0·146, 0·035, 0·014	0·14	0·289

gl, glass; ol, olivine; opx, orthopyroxene; cpx, clinopyroxene; aug, augite; gar, garnet; sp, spinel; [], relict mineral; plag, plagioclase; pig, pigeonite. RSSQ, residual sum of squares in regression of phase proportions. $K_D^{opx-liq} = [(FeO)^{opx}/(FeO)^{liq}] \times [(MgO)^{liq}/(MgO)^{opx}]$.
*Weight fraction of phases in order listed under 'run products'; where available, analyzed bulk compositions (Table 1) are used in the regressions.
†Negative opx compensates for relic olivine that is not included in the regressions.

Table 3: Composition of phases in weight percent oxides

Run	Phase	Pts*	SiO_2	TiO_2	Al_2O_3	Cr_2O_3	FeO	MgO	MnO	CaO	K_2O	Na_2O	P_2O_5	Sum
HLOL-3	liq	5	47·6(3)†	2·43(5)	17·8(2)	0·01(1)	13·0(1)	5·57(9)	0·12(2)	7·45(5)	0·78(2)	3·88(15)	0·25(2)	98·8
	opx	6	50·1(1·1)	0·49(9)	8·78(1·57)	0·06(2)	14·2(5)	24·4(7)	0·14(1)	1·94(11)		0·18(1)		100·3
	cpx	7	49·2(4)	0·85(7)	9·74(25)	0·07(3)	11·7(3)	16·8(5)	0·16(4)	10·8(4)		0·87(4)		100·1
	sp	4	46(16)	0·46(4)	62·4(7)	0·83(41)	18·8(2)	17·2(3)	0·06(1)	0·14(3)		0·02(1)		100·3
HLOL-4	liq	8	46·1(2)	1·97(3)	17·4(1)	0·03(3)	12·5(1)	7·80(5)	0·15(2)	8·67(7)	0·58(2)	3·08(5)	0·19(1)	98·5
	cpx	18	49·1(7)	0·66(6)	8·56(41)	0·08(4)	10·5(4)	19·6(8)	0·16(2)	9·08(87)		0·55(5)		98·3
	opx	3	51·6(1·2)	0·37(8)	6·46(2·15)	0·10(2)	12·1(3)	26·1(7)	0·13(2)	2·27(7)		0·15(1)		99·3
	sp	6	0·27(9)	0·40(13)	63·0(1·4)	1·51(1·05)	15·3(4)	19·0(5)	0·10(2)	0·10(3)		0·01(1)		99·6
HT80E-1	liq	6	48·0(0)	1·29(3)	18·3(1)	0·01(1)	12·7(2)	5·58(4)	0·15(1)	7·89(6)	0·60(4)	3·55(8)	0·22(6)	98·3
	cpx	9	47·3(8)	0·58(7)	12·3(1·2)	0·02(1)	11·4(5)	15·2(5)	0·20(2)	11·3(1·1)		0·85(5)		99·3
	opx	7	49·3(8)	0·35(8)	11·0(1·0)		15·0(3)	23·4(5)	0·22(1)	2·05(26)		0·18(2)		101·5
	opx‡	1	52·9(0)	0·20(0)	8·42(0)		10·3(0)	28·3(0)	0·19(0)	2·21(0)		0·13(0)		102·7
	ol‡	1	38·0(0)	0·00(0)	0·00(0)	0·04(0)	27·6(0)	36·2(0)	0·24(0)	0·26(0)		0·03(0)		102·4
	sp	6	0·18(10)	0·21(1)	65·8(1·5)	0·39(36)	18·2(1)	17·1(2)	0·10(2)	0·07(3)		0·01(1)		102·0
	plag	10	54·8(8)		29·0(5)		0·43(4)	0·16(17)		11·4(6)	0·24(6)	4·98(26)		101·0
HT80E-4	liq	5	48·2(1)	1·19(3)	18·5(1)	0·01(1)	11·6(1)	5·77(6)	0·12(1)	8·56(7)	0·51(0)	3·62(6)	0·23(1)	98·3
	gar	6	40·2(5)	0·63(11)	23·9(1)	0·03(2)	14·2(2)	15·0(3)	0·33(1)	6·48(18)		0·02(1)		100·8
	cpx	7	47·4(6)	0·54(8)	13·1(5)	0·02(2)	8·18(59)	13·7(2)	0·14(1)	15·1(6)		1·08(5)		99·2
	plag	12	52·8(1·4)	0·03(2)	29·5(9)		0·49(8)	0·09(3)		12·3(1·0)	0·21(5)	4·24(57)		99·6
HT80E-5	liq	6	47·2(3)	1·37(7)	17·8(1)	0·02(1)	13·3(1)	6·09(5)	0·18(2)	8·44(7)	0·51(2)	3·40(8)	0·23(2)	98·5
	aug	10	48·6(8)	0·68(20)	10·1(1·0)	0·03(2)	10·7(6)	16·0(7)	0·20(3)	12·6(9)		0·73(14)		99·6
	opx	4	49·7(8)	0·45(22)	9·31(1·24)	0·00(0)	13·9(5)	24·1(8)	0·19(1)	2·04(10)		0·11(2)		99·9
	pig	1	49·7(0)	0·41(0)	7·96(0)	0·00(0)	14·0(0)	21·8(0)	0·23(0)	4·50(0)		0·21(0)		98·9
	plag	11	53·1(1·3)	0·04(2)	29·3(8)		0·48(6)	0·09(2)		12·1(9)	0·24(5)	4·31(44)		99·6
HT80E-6	liq	8	49·4(5)	1·53(4)	18·4(1)	0·00(0)	11·1(1)	3·81(5)	0·07(1)	6·45(5)	1·17(4)	5·21(12)	0·53(4)	97·6
	cpx	8	48·2(4)	0·94(8)	12·0(7)	0·02(1)	9·98(74)	11·9(5)	0·14(3)	14·5(8)		1·47(6)		99·2
	gar	5	40·0(3)	0·71(14)	22·5(2)	0·03(1)	17·4(3)	12·4(2)	0·29(2)	6·65(11)		0·02(1)		100·0
	plag	6	57·0(4)	0·08(1)	27·3(2)		0·46(8)	0·07(2)		9·06(20)	0·36(2)	5·75(14)		100·1
HT80E-7	liq	7	46·8(2)	1·09(4)	18·0(0)	0·01(1)	12·2(1)	6·88(4)	0·14(2)	9·11(7)	0·40(3)	3·10(8)	0·19(1)	98·0
	opx	6	50·0(6)	0·27(3)	9·06(52)	0·02(1)	12·4(3)	25·0(3)	0·18(1)	2·14(15)		0·10(1)		99·1
	sp	5	0·06(8)	0·19(2)	65·9(1·2)	0·18(5)	15·2(2)	17·2(3)	0·10(1)	0·07(2)		0·00(0)		98·0
	plag	6	52·1(4)	0·06(1)	29·7(2)		0·43(10)	0·16(3)		12·5(2)	0·15(2)	3·99(14)		99·1
HT/HL-1	liq	6	48·0(1)	1·29(3)	18·3(1)	0·01(1)	12·7(2)	5·58(4)	0·15(1)	7·89(6)	0·60(4)	3·55(8)	0·22(6)	98·3
	opx	9	49·2(51)	0·38(5)	9·47(92	0·12(6)	14·9(3)	23·4[3)	0·20(3)	2·05(23)		0·12(1)		99·8
	cpx	5	48·8(8)	0·65(12)	9·94(97)	0·13(2)	11·6(9)	16·4(1·4)	0·22(2)	10·9(1·8)		0·6911)		99·5
	plag	10	54·1(1·1)	0·00(0)	29·3(7)		0·55(6)	0·13(2)		11·8(8)	0·20(3)	4·77(52)		100·8
HLCA-25	liq	6	49·0(2)	2·33(7)	16·6(1)	0·01(1)	12·4(1)	5·27(6)	0·17(1)	8·23(5)	0·62(4)	2·98(11)	0·19(2)	97·9
	cpx§	8	48·6(7)	0·76(9)	9·75(82)	0·21(6)	13·1(8)	16·7(9)	0·23(2)	9·65(1·42)		0·61(10)		99·6
	opx	5	49·7(5)	0·50(5)	9·06(58)	0·25(9)	15·5(7)	22·2(5)	0·19(3)	2·29(45)		0·15(2)		99·9
	plag	10	54·5(1·0)	0·11(1)	27·8(4)		0·71(5)	0·11(2)		10·8(5)	0·27(2)	4·92(26)		99·3

with respect to the crystalline phases in contact with liquid. For example, sample HT80E is a troctolite, but olivine is clearly not stable in any of the runs at 10–13 kbar, thus demonstrating the instability of olivine in plagioclase-saturated liquids of this general type at pressures $\geq$10 kbar. On the other hand, neither aluminous spinel nor garnet is present in the starting rock material, yet they grow readily and mutually exclusively at 10–11·5 and 13 kbar, respectively. Furthermore, the Fe–Mg exchange coefficient (K_D) for orthopyroxene–liquid pairs (Table 2) has a limited range of values that is approximately the same for isothermal experiments with devitrified glass starting material (0·297–0·249) as it is for polythermal experiments or those with powdered rock starting material (0·281–0·259). These observations are consistent with our previous work based on reversals of plagioclase and orthopyroxene compositions, demonstrating that isothermal experiments on devitrified glass starting materials produced equilibrium phase assemblages and compositions (mantles, rims) in runs with

Run	Phase	Pts*	SiO_2	TiO_2	Al_2O_3	Cr_2O_3	FeO	MgO	MnO	CaO	K_2O	Na_2O	P_2O_5	Sum
HLCA-44	liq	4	45·8(1·1)	4·00(42)	12·2(1·5)	0·00(0)	20·9(1·3)	4·30(75)	0·23(2)	7·47(60)	1·12(31)	3·42(82)	0·35(5)	99·8
	pig	8	52·0(4)	0·71(7)	3·23(47)	0·14(4)	16·9(2)	21·8(4)	0·30(2)	3·95(47)		0·16(4)		99·2
	plag	4	53·8(6)	0·28(9)	28·7(4)		1·20(33)	0·43(11)		11·6(34)	0·36(12)	4·48(8)		100·9
HLCA-53	liq	4	48·1(3)	2·74(5)	15·4(1)	0·15(2)	12·7(1)	5·94(5)	0·34(1)	8·41(7)	0·69(9)	3·56(7)	0·40(1)	98·4
	opx	16	52·9(5)	0·83(4)	4·70(69)	0·35(5)	14·2(4)	25·6(4)	0·38(3)	2·26(28)		0·15(2)		101·4
	pig	1	53·3(0)	0·40(0)	2·99(0)	0·28(0)	14·1(0)	26·2(0)	0·28(0)	3·72(0)		0·15(0)		101·4
	ol	3	38·3(0)	0·07(3)	0·10[4)	0·03()	25·7(4)	37·4[6)	0·28(1)	0·36(4)				102·2
	plag	7	53·5(5)	0·09(2)	30·0(3)		0·46(4)	0·12(1)		12·4(2)	0·19(3)	4·38(15)		101·1
HLCA-55	liq	5	48·8(2)	2·59(1)	17·2(1)	0·14(2)	12·1(2)	5·56(5)	0·29(3)	8·43(3)	0·67(4)	3·06(16)	0·39(2)	99·2
	cpx	3	49·1(1·1)	0·71(4)	8·93(31)	0·24(6)	12·1(5)	17·0(3)	0·23(4)	11·6(7)		0·68(2)		100·6
	opx	11	51·0(5)	0·31(13)	8·06(42)	0·26(8)	14·8(7)	24·4(2)	0·22(3)	2·20(13)		0·16(2)		101·5
	plag	12	54·7(4)	0·03(1)	28·8(3)		0·50(9)	0·13(3)		11·4(1)	0·20(4)	4·60(20)		100·4

Abbreviations as in Table 2. Blanks indicate element not analyzed.
* Number of spots or areas analyzed.
† Units in parentheses are 1 SD of replicate analyses in terms of least unit(s) cited.
‡ Relict mineral grain.
§ Possibly two near-critical clinopyroxenes present.

$\geq 60\%$ liquid on a time scale of 1–2 days (Longhi *et al.*, 1993). Therefore, we are confident of the reported phase assemblages and liquid compositions in all of the runs, but would caution against the use of crystal–liquid partitioning data derived from runs with $\leq 60\%$ liquid or from polythermal runs.

RESULTS

Although we have new data at several pressures, the most complete set is for the HLCA series at 11·5 kbar. Accordingly, we will illustrate these data first, and then go on to examine the effects of pressure and composition. The compositions of coexisting crystals and liquids from the HLCA series at 11·5 kbar are shown in two projections of the quartz–olivine–plagioclase–wollastonite (Qtz–Ol–Pl–Wo) system (Longhi, 1991) in Fig. 1. The HLCA series liquids have the characteristics expected of moderately evolved basalts: intermediate *mg*-number (0·5–0·4) and intermediate normative feldspar ($Ab_{40-50}Or_5$). Although the liquids in this figure are not saturated with ilmenite, the compositions are projected from an Ilmenite component ($[Fe,Mg]TiO_3$) for the sake of consistency with subsequent figures, which illustrate jotunitic compositions that are saturated with ilmenite. In this figure and in those that follow, we will try to limit the range of *mg*-number and normative feldspar composition as much as possible. This means that the diagrams are a useful means of predicting phase saturation and the nature of invariant points for a family of compositions, but because the liquidus boundaries shift with composition, the fractionation paths of individual compositions will in general diverge from the depicted liquidus boundaries [see fig. 5 of Longhi (1991)]. Also, because it is not feasible to make *mg*-number and normative feldspar composition precisely constant everywhere even with multiple bulk compositions, it is inevitable that low-temperature portions of some liquidus boundaries may have been defined with experimental liquids having higher *mg*-number or more anorthitic normative feldspar than liquids used to define the ostensibly higher temperature portions of the same or a related boundary. Thus it is possible that the reported temperatures of some of the experimental liquids may apparently violate the direction of falling temperature inferred from the topology of the coexisting phases. In such cases, the reader should keep in mind that the boundary curves are not strictly isobaric-univariant, and topology takes precedence.

Figure 1a illustrates the array of liquidus boundaries saturated with augitic clinopyroxene. Projecting from the Wollastonite ($Wo = CaSiO_3$) component rather than Diopside is useful when clinopyroxene (*cpx*) is a late-crystallizing phase in the experiments, because the Wo projection causes less parallax dispersion of the subjacent, clinopyroxene-absent liquidus surfaces, e.g. the olivine (*ol*) + plagioclase (*plag*) liquidus surface projects as a narrow band under the *ol* + *plag* + *cpx* liquidus boundary curve rather than as a broad band off to the side [see fig. 10 of Longhi (1987)]. This feature makes the Wo projection useful in representing the limits of the primary liquidus volumes of compositions with relatively low Wo contents. Pyroxene compositions in Fig. 1a plot approximately on the trace of the Orthopyroxene ($Opx = [Mg,Fe]_2Si_2O_6$)–Mg-Tschermak ($[Mg,Fe]Al_2SiO_6$) join,

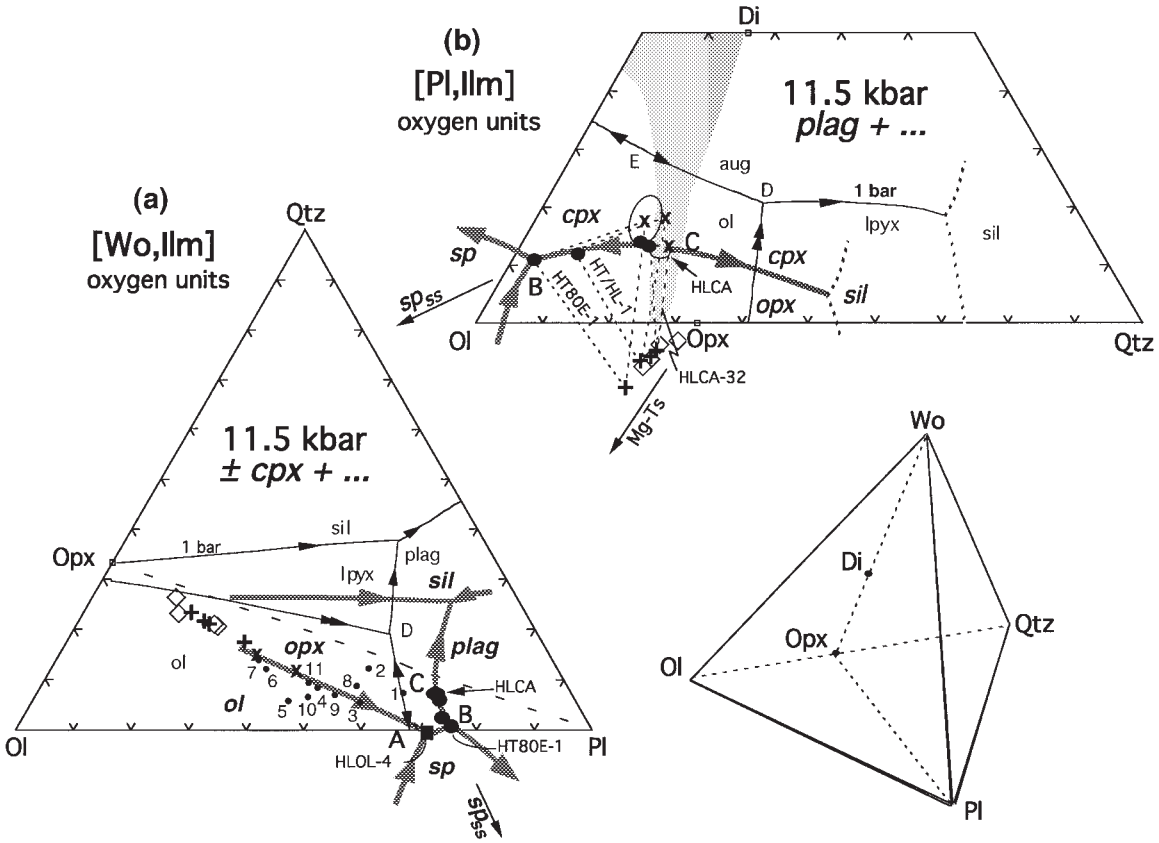

Fig. 1. Liquidus equilibria at 11·5 kbar projected into the model system olivine–plagioclase–wollastonite–ilmenite–orthoclase–quartz (Ol–Pl–Wo–Ilm–Or–Qtz) in terms of oxygen units, modified after Longhi (1991). (a) Subprojection of clinopyroxene-saturated and -undersaturated liquidus boundaries from the Wo, Or and Ilm components onto the plane Ol–Pl–Qtz. (b) Subprojection of plagioclase-saturated liquids and crystals from the Pl, Or and Ilm components onto the Ol–Qtz–Wo plane. Light continuous lines show augite-saturated and plagioclase-saturated liquidus boundaries at 1 bar calculated for HLCA-like compositions (*mg*-number = 0·52, NAb = 0·42, NOr = 0·04) from the algorithms of Longhi (1991). Bold lines show 11·5 kbar liquidus boundaries based on data from Fram & Longhi (1992) and this study. Arrows show direction of decreasing temperature; double arrows indicate a reaction boundary. '*sil*' refers to silica phase—cristobalite, tridymite, or quartz. Experimental data: ●, *liq* (+ *aug* + *lpyx* + *plag*); ■, *liq* (+ *aug* + *lpyx* + *sp*); ○, *liq* (+ *lpyx* + *plag*); ×, *cpx*; +, *opx*; ◇, *opx* megacryst compositions with *mg*-number ≥0·70 from Emslie (1980) and Maquil & Duchesne (1984). Numbered dots are primitive magma compositions from Basaltic Volcanism Study Project (BVSP) (1981): 1 and 2, mid-ocean ridge basalt (MORB) (cols 1 and 4, table 1.2.5.3); 3–7, continental flood basalts (Svartenhuk and Baffin Island *ol*-tholeiites, table 1.2.3.7; cols 15 and 16, table 1.4.2.1; col. 2, table 1.2.2.10); 8 and 9, Hawaiian tholeiites (cols 1 and 2, table 1.2.6.14); 10, Gorgona basaltic komatiite (col. 9, table 1.4.2.1); 11, high-Mg ophiolite dike (col. 11, table 1.2.5.3). Shaded area is the range of clinopyroxene solid solution. Ellipse shows the range of *cpx* analyses in run HT80E-1. Dashed lines connect coexisting phases. A, B, C, D, E are pseudo-invariant points described in the text. Projection equations, oxygen units:

$$\mathrm{Ol[Wo,Ilm]} = 2(\mathrm{FeO} + \mathrm{MgO} + \mathrm{MnO} - \mathrm{TiO_2})/\Sigma\mathrm{[Wo,Ilm]}$$
$$\mathrm{Pl[Wo,Ilm]} = 8(\mathrm{Al_2O_3} + \mathrm{Na_2O} - \mathrm{K_2O})/\Sigma\mathrm{[Wo,Ilm]}$$
$$\mathrm{Qtz[Wo,Ilm]} = [2\mathrm{SiO_2} - (\mathrm{FeO} + \mathrm{MgO} + \mathrm{MnO} - \mathrm{TiO_2}) - 2\mathrm{Al_2O_3} - 2\mathrm{CaO} - 10(\mathrm{Na_2O} + \mathrm{K_2O})]/\Sigma\mathrm{[Wo,Ilm]}$$
$$\mathrm{Ol[Pl,Ilm]} = 2(\mathrm{FeO} + \mathrm{MgO} + \mathrm{MnO} - \mathrm{TiO_2})/\Sigma\mathrm{[Pl,Ilm]}$$
$$\mathrm{Wo[Pl,Ilm]} = 3(\mathrm{CaO} - \mathrm{Al_2O_3} + \mathrm{Na_2O} + \mathrm{K_2O})/\Sigma\mathrm{[Pl,Ilm]}$$
$$\mathrm{Qtz[Pl,Ilm]} = [2\mathrm{SiO_2} - (\mathrm{FeO} + \mathrm{MgO} + \mathrm{MnO} - \mathrm{TiO_2}) - 2\mathrm{Al_2O_3} - 2\mathrm{CaO} - 10(\mathrm{Na_2O} + \mathrm{K_2O})]/\Sigma\mathrm{[Pl,Ilm]}$$

where [Wo,Ilm] and [Pl,Ilm] identify the main projection components, Σ[Wo,Ilm] and Σ[Pl,Ilm] refer to the sums of the right-hand sides of the equations, and the oxides are mole fractions.

which crosses the base of the triangle at $Ol_{0·333}Pl_{0·667}$. Figure 1b illustrates a more conventional projection from the Plagioclase and Ilmenite components [Pl,Ilm] of phase relations on the plagioclase liquidus surface. The compositions of clinopyroxene coexisting with orthopyroxene (*opx*) and/or spinel (*sp*) define the limits of the

shaded *cpx* solid solution field. Pyroxene phase relations are rather complex for the compositions considered here: at pressures ≥ 10 kbar clinopyroxenes in HLCA-like composition appear to have a continuous (or nearly so) range of composition between Di and Opx; whereas at lower pressures (see below) distinct high- and low-Ca clinopyroxenes are stable. Following the convention of Longhi & Bertka (1996), we will refer to apparently hypersolvus clinopyroxene as *cpx*, and reserve the terms augite (*aug*) and pigeonite (*pig*) for subsolvus clinopyroxene. Where the *cpx* solid solution is not continuous, there may be two closely spaced liquidus curves involving two pyroxenes for liquids with intermediate *mg*-number, *opx* + *pig* + *plag* and *pig* + *aug* + *plag*; whereas for more magnesian or more ferroan compositions there may be only one two-pyroxene curve, *opx* + *aug* + *plag* (*pig* stable only in *plag*- undersaturated liquids) or *pig* + *aug* + *plag* (*opx* unstable), respectively [see Longhi (1991)]. To avoid unnecessary complexity, we will depict only one two-pyroxene liquidus curve at a time, and we will refer to low-Ca pyroxene (*lpyx*) to signify either *opx* or *pig*. In Fig. 1 and subsequent figures the compositions of all clinopyroxenes are represented with a '×', whereas orthopyroxene is marked by a '+'.

The new data plus data from Bartels *et al.* (1991) and Kinzler & Grove (1992) constrain the nature of three pseudo-invariant points involving olivine, orthopyroxene, clinopyroxene, plagioclase, and aluminous spinel. One is a *plag*-absent *ol* peritectic (A): *liq* + *ol* = *opx* + *cpx* + *sp*. The second is an *ol*-absent *opx* peritectic (B): *liq* + *opx* = *cpx* + *plag* + *sp*. The third is a thermal maximum (C) on the *plag* + *opx* + *cpx* liquidus boundary where the compositions of crystals and liquid are coplanar (note the coplanar arrangement can be adequately depicted only in the [Pl,Ilm] projection). Even though the *cpx* compositions in runs HT80E-1 and the HT/Hl-1 do not define tight limits on *cpx* solid solution (because of incomplete equilibration of the clinopyroxene in the charges containing natural rock powders), the data for these runs plus HLCA-32 (Fram & Longhi, 1992) describe three three-phase triangles with the *liq* corners pointing away from Qtz. However, the HLCA-32 three-phase triangle is nearly collapsed to the *opx* + *cpx* tieline. It should be obvious, therefore, that an apparent collinearity of coexisting pyroxenes and liquid occurs on the *plag* + *opx* + *cpx* liquidus boundary slightly to the right of the HLCA-32 liquid point and that a set of three-phase triangles pointing toward Qtz must exist for liquids on this curve to the right of the Opx–Di join. The locus of the apparent collinearity on the boundary curve is a thermal maximum and has a temperature ≥ 1275°C (run HLCA-32) for liquids with similar *mg*-number and alkalis. Baker & Eggler (1987; fig. 5) have demonstrated the existence of this thermal maximum in melts of calc-alkaline basalts at 8 kbar and their data are illustrated below.

The nature of point A is well known from other studies (e.g. Kinzler & Grove, 1992), but may be partially inferred by noting that in Fig. 1a the compositions of liquid, orthopyroxene, olivine, and spinel describe the corners of an irregular quadrilateral with liquid and olivine at opposite corners. Analogously, the *opx* + *liq* reaction at point B may be inferred in Fig. 1b by observing that the coexisting *opx* and *liq* compositions lie at opposite corners of a quadrilateral with the *aug* and *sp* compositions at the other two corners.

The array of liquidus curves constrains the crystallization paths of basaltic magmas and the permissible range of crustal melts. Initially *ol*-saturated liquids, crystallizing either *ol* + *opx* + *cpx* or *ol* + *cpx* + *sp*, will reach point A (Fig. 1a), react out olivine, and crystallize an interval of *opx* + *cpx* + *sp* before reaching point B. It is possible that for some compositions *opx* will be in reaction with liquid between A and B (*opx* + *liq* → *cpx* + *sp*)—it should be noted in Table 2 that the proportion of *opx* decreases between 1300°C (HLOL-4) and 1265°C (HLOL-3)—so some fractionating liquids may reach *plag* saturation with only *cpx* stable. At B any orthopyroxene reacts out and further crystallization proceeds along the *cpx* + *plag* + *sp* cotectic, away from the Qtz and Opx components. In this way it is possible to produce high-Al_2O_3 liquids (≥ 18 wt % Al_2O_3) that are also nepheline-normative (liquids that lie to the low-silica side of the Ol–Di join in Fig. 1b) and a series of cumulates that begin with either spinel wehrlite or olivine pyroxenite, followed by spinel pyroxenite (A → B), and then spinel gabbro. The data of Kinzler & Grove (1992) and Walter & Presnall (1994) show that for liquids with similar normative feldspar, but higher *mg*-number, all five crystalline phases may coexist with liquid. In these cases, three dimensions are not adequate to represent the liquidus boundaries as curves; and, instead of the *liq* + *opx* + *cpx* + *sp* curve joining the ol and plag surfaces, portions of the ol and plag surfaces will overlap with a smeared-out combination of points A and B (*liq* + *ol* + *opx* + *cpx* + *sp*) joining plag-free portions of the *ol* saturation surface to *ol*-free portions of the *plag* saturation surface. The net result of these two topologies is similar: initially *ol*-saturated, fractionating liquids will eventually wind up on the *ol*-absent portion of the *plag* saturation surface. Because of the plagioclase + pyroxene thermal divide (C), however, there is no way for a fractionating basaltic liquid to move toward the Qtz component. Conversely, low-degree melts of crustal rocks containing plagioclase and orthopyroxene may access a wide range of Qtz contents. Such melts are restricted to only the vicinity of the *plag* + *opx* + *cpx* liquidus boundary, which extends from high-SiO_2 granitic compositions

at silica saturation to high-Al_2O_3, nepheline-normative compositions at spinel saturation.

To discuss crystallization and melting paths throughout the crust, we must first understand how the topologies shown in Fig. 1 change with pressure. The topologies of the *aug* and *plag* saturation surfaces are well known at 1 bar over a range of composition (e.g. Grove & Juster, 1989; Longhi, 1991), so intermediate topologies between 1 bar and 11·5 kbar may be interpolated and successive topologies extrapolated to higher pressures. Once a given topology is recognized, its compositional and pressure range may even be constrained by a single key experimental datum. In this way a progression of phase diagrams has been constructed from 1 bar to 13 kbar and illustrated in Fig. 2 for liquids with the same general character (intermediate *mg*-number and normative feldspar) as those in Fig. 1. Figure 3 illustrates a similar set of constructions for jotunitic liquids, which have lower *mg*-number (0·4–0·25) and more alkaline normative feldspar ($Ab_{50–65}Or_{9–20}$). The bulk compositions of HLCA and TJ are plotted for reference in all panels of Figs 2 and 3, respectively.

The progressions of topologies in Figs 2 and 3 are relatively similar: in the [Wo,Ilm] projections (Figs 2a and 3a) the major features are the shift of the *ol* + *lpyx* + *aug* + *liq* boundary away from the Qtz component with increasing pressure (where *lpyx* signifies orthopyroxene and/or pigeonite); whereas in the [Pl,Ilm] projections (Figs 2b and 3b) the major feature is the shift of the *ol* + *lpyx* + *plag* + *liq* boundary away from Qtz. In both projections the *lpyx* and *sp* saturation surfaces eventually intersect and with still higher pressure garnet (*gar*) replaces spinel. At 1 bar the *ol* + *plag* + *lpyx* + *aug* + *liq* pseudo-invariant point (D) is an *ol* peritectic and there is a thermal maximum on the *ol* + *plag* + *aug* + *liq* boundary (E) that separates liquids that may fractionate to lpyx saturation from those that fractionate toward nepheline saturation. By 5 kbar, point D has migrated across the pyroxene–plagioclase plane (the trace of Opx–Pl in Figs 2a and 3a or the Opx–Di join in Figs 2b and 3b). This movement precipitates two changes: first, a thermal maximum (C) is exposed on the *lpyx* + *aug* + *plag* + *liq* boundary curve where the liquid composition appears to be collinear with those of the coexisting *lpyx* and *aug*; and second, because the *ol* + *plag* + *lpyx* + *aug* + *liq* pseudo-invariant point (D) now lies between two thermal maxima, D must be a eutectic. If the *ol* + *plag* + *lpyx* + *liq* boundary is curved as shown in Figs 2b and 3b, then the boundary curve crosses the line of pyroxene solid solutions at an angle, which enables olivine to be in reaction with liquid along the low Wo portion of the curve and to crystallize from liquids along the high Wo portion of the boundary. Thus at the same pressure there can be similar liquids, differing only slightly in Wo content, with very different crystallization paths: one that produces marked silica enrichment and *qtz*-bearing assemblages, whereas the other produces little or no silica enrichment and *ol*-bearing assemblages. These paths will be illustrated below.

By 6 kbar (Figs 2b and 3b) point D has overtaken the *ol* + *plag* + *aug* + *liq* thermal maximum (E). Once it does, the *ol* + *plag* + *aug* + *liq* thermal maximum (E) disappears and the equilibrium relations at point D must necessarily change to an *opx*(*lpyx*) peritectic (Fig. 2b, 8 kbar). With further increases in pressure, the *lpyx* and *sp* fields intersect (~10 kbar) and separate the *ol* and *plag* liquidus fields as described above, generating pseudo invariant points A and B (see Fig. 1a). The disposition of coexisting *cpx*, *opx*, *sp*, and *liq* (B) compositions at 10 and 11·5 kbar in Fig. 2b is also quadrilateral and, thus, B remains an *opx*(*lpyx*) peritectic. By 13 kbar garnet has replaced spinel in pyroxene-saturated liquids on the plagioclase surface; but none the less, the new pseudo-invariant point involving garnet (B′) remains an *opx* peritectic. Other important shifts in liquidus boundaries with increasing pressure include movement of the *plag* + *lpyx* + *aug*/*cpx* liquidus boundary away from Wo in the [Pl,Ilm] projections and away from Opx in the [Wo, Ilm] projections. The movement of the *plag* + *lpyx* + *aug* liquidus boundary away from Opx in the [Wo,Ilm] projections is apparently much greater in high- than in low-silica compositions such that an inflection of the curve occurs in the vicinity of the plagioclase + pyroxene thermal divide.

Although these shifts in liquidus boundaries are general features of basalts, the shifts are compositionally dependent. Specifically, for liquids with higher *mg*-number the boundary curves involving olivine and low-Ca pyroxene project at higher Qtz contents and the *lpyx* + *augite* boundary lies at higher Wo, as illustrated in Fig. 2 with 10 kbar data (dashed lines) from Bartels *et al.* (1991; run H142). Consequently, the transitions in topology described above take place at higher pressures in more magnesian liquids and, in extreme cases, may not occur at all. For example, the data from run H130 [*mg*-number(*liq*) = 0·64] of Kinzler & Grove (1992) show the transition of point D from a eutectic to an *opx* peritectic occurring at 9 kbar (their fig. 1) vs at ~6 kbar for the less magnesian compositions of the present study, whereas, in the CMAS system, the data of Presnall *et al.* (1979) and Walter & Presnall (1994) show that point D crosses neither the Ol–Pl–Di join nor the line of coexisting *opx* and *aug* (diopside); consequently, D remains an *ol* peritectic until spinel separates the liquidus volumes of olivine and anorthite at 9·3 kbar. The *mg*-number value of 0·64 from run H130 is a likely upper limit to the *mg*-number of *plag*-saturated liquids at lower-crustal pressures because ascending mantle-derived melts are likely to be saturated only in olivine and will thus require moderate

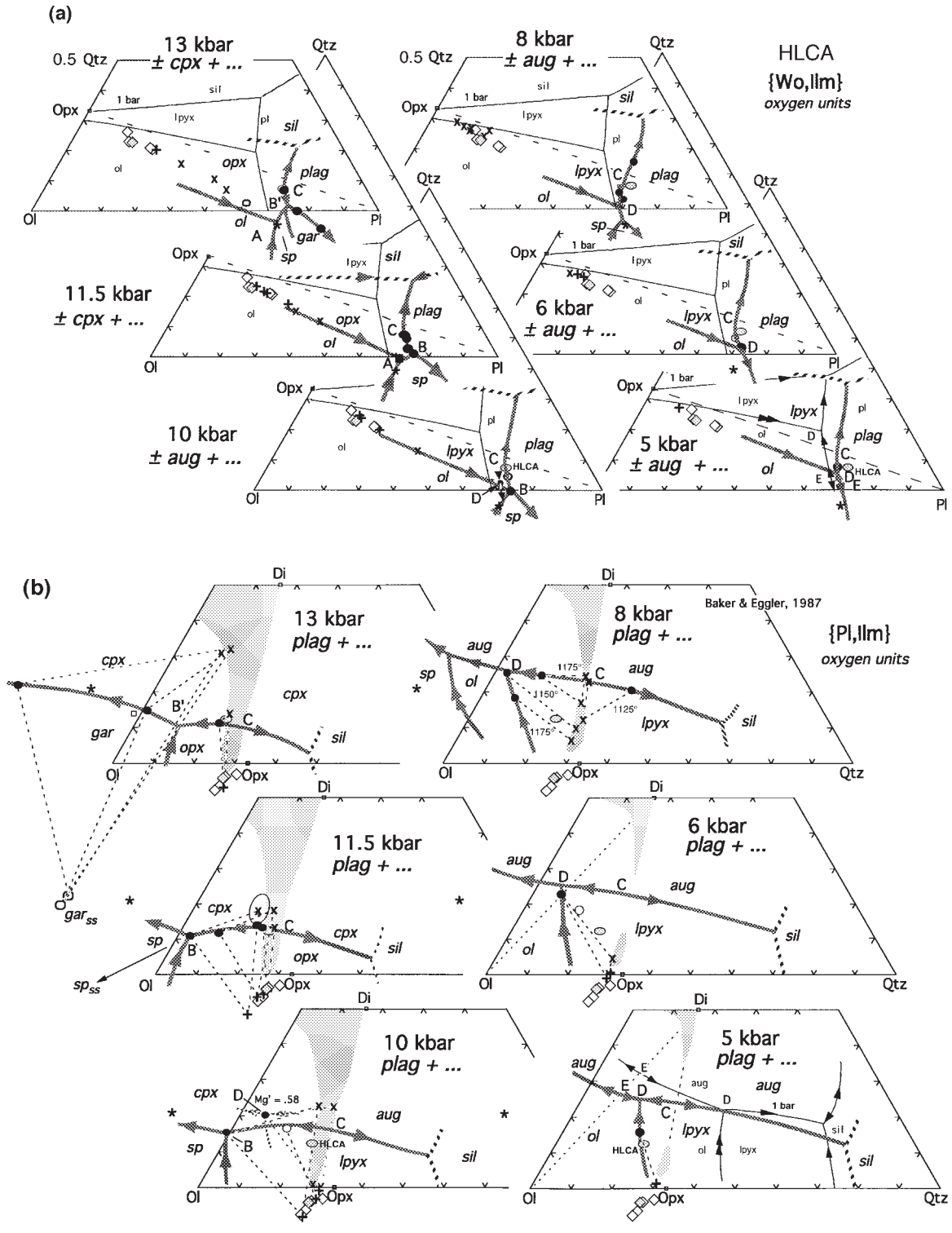

Fig. 2. Progression of liquidus equilibria and solid solutions for HLCA-like compositions from 1 bar to 13 kbar. Projection schemes as in Fig. 1. Light solid lines in 5 kbar panel are 1 bar liquidus boundary curves. ●, *liq* (+ *aug*/*cpx* + *lpyx* + *plag*) or *liq* (+ *ol* + *lpyx* + *plag*); blunted ellipses are garnet compositions; ○, *liq* (+ *lpyx* + *plag*); shaded areas indicate estimated limits of clinopyroxene solid solution; dashed curves indicate estimated positions of liquidus boundaries; shaded diamond, HAOM 860C from Wiebe (1986); *, host dike 860C from Wiebe (1985) with $Fe^{3+}/Fe^{tot} = 0{\cdot}1$; otherwise symbols as in Fig. 1. The 8 kbar data are from Baker & Eggler (1987); 10 kbar high *mg*-number data are run H142 from Bartels *et al.* (1991); rest of experimental data from Fram & Longhi (1992) and this study.

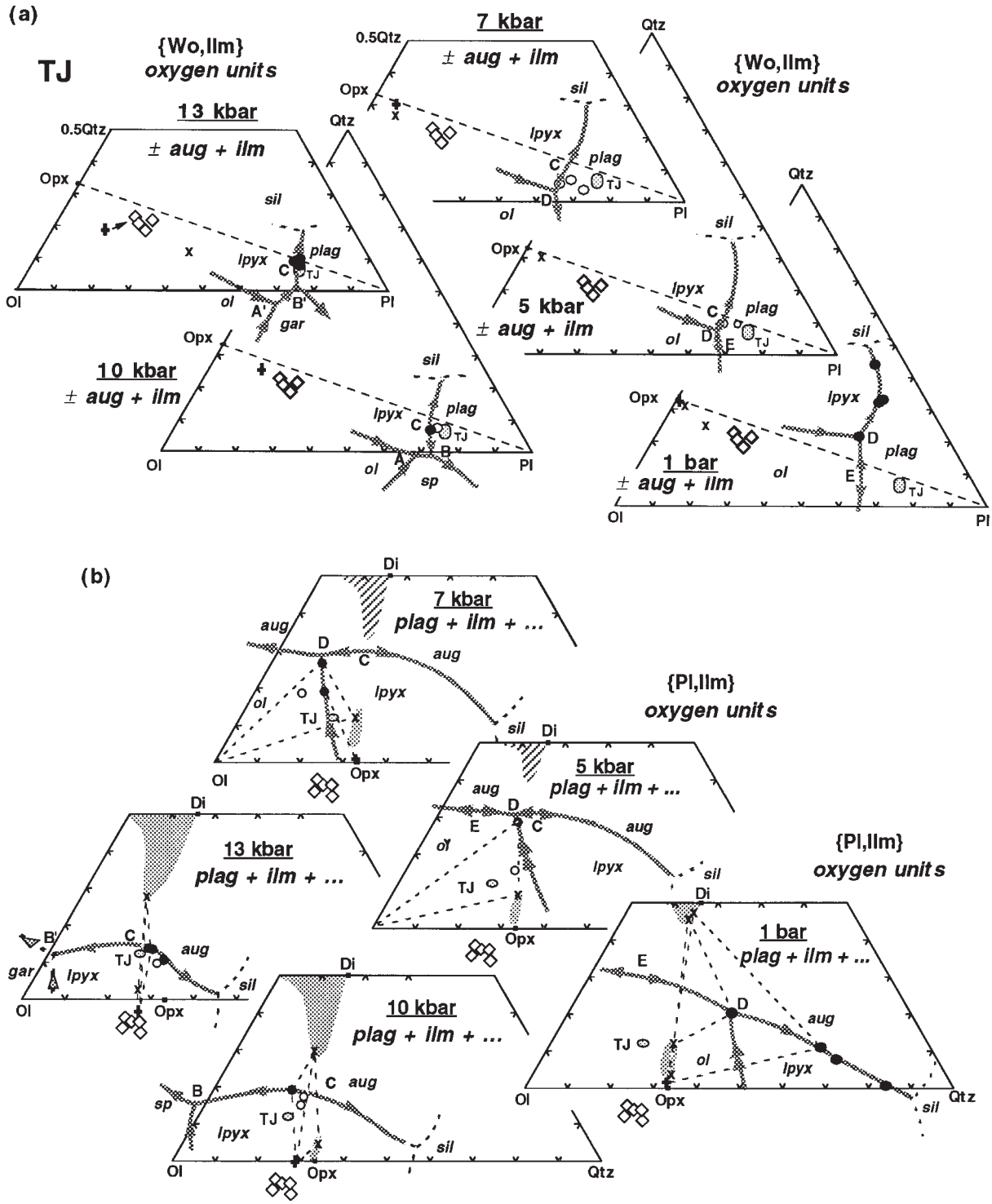

Fig. 3. Progression of liquidus equilibria and solid solutions for TJ-like compositions from 1 bar to 13 kbar. Projection schemes as in Fig. 1. Data from Vander Auwera & Longhi (1994). All liquids are near or at ilmenite saturation. The 1 bar liquids include runs at FMQ – 1, low Qtz, *mg*-number(*liq*) = 0·25, and at NNO (nickel–nickel oxide), high Qtz, *mg*-number(*liq*) = 0·42–0·33. The higher *mg*-number in the NNO liquids produces a relative expansion of the *lpyx* + *liq* field that is responsible for the strong curvature of the *lpyx* + *aug* + *plag* liquidus boundary. Diamonds are Rogaland megacryst compositions from Duchesne & Maquil (1987).

crystallization of olivine and probably pyroxene before reaching plagioclase saturation. For example, the compositions of several proposed parental (if not primary) liquids with *mg*-number ranging from 0·63 to 0·76 (BSVP, 1981) are shown as numbered dots in Fig. 1a. These compositions include primitive MORB (1 and 2), picritic flood basalts (3–7), parental Hawaiian tholeiites (8 and 9), Gorgona basaltic komatiite (10), and a high-Mg ophiolite dike (11). Because the *ol* + *opx* ± *cpx* liquidus boundary shifts away from the Ol component as *mg*-number increases, all of these magnesian compositions except the two MORBs will be saturated with *ol* ± *opx* ± *cpx* at 11·5 kbar and will evolve toward the vicinity of point A along their respective *ol* + *opx* + *cpx* boundary curves. Crystallization calculations based upon the pressure-dependent algorithms of Longhi (1992) indicate that the liquids derivative to compositions 3–11 at 11·5 kbar will all have *mg*-number ≤ 0·60 upon reaching point A. Thus, the *mg*-number values of compositions like HLCA (0·51), TJ (0·45), and those of the experimental liquids along the *plag* saturation surface are consistent with values expected of even more evolved liquids.

The two MORB compositions, which project well into the *opx* liquidus field at 11·5 kbar, represent equilibration along the *ol* + *opx* + *cpx* liquidus boundary at 8–9 kbar. Thus the crystallization paths of these primitive MORBs cannot be considered to be representative of mantle-derived liquids at 11·5 kbar. However, at 8 kbar, where these compositions do represent plausible mantle-derived liquids, their derivatives would probably reach *plag* saturation with sufficiently high *mg*-number that D would be eutectic-like. But with continued crystallization *mg*-number would fall into the range appropriate for Fig. 2 (≤0·5); and as *mg*-number decreased, the composition of D would migrate away from Qtz and Wo until it crossed the plane of coexisting *ol*, *aug*, and *plag* compositions, at which point D would become a nepheline-normative *opx* peritectic—consistent with Fig. 2. Thus the differentiates of primitive MORBs at 8 kbar would ultimately become nepheline-normative and react out *opx*, even though they may have initially encountered eutectic-like equilibria at D.

As liquidus boundaries are shifting in response to increasing pressure, the solid solution limits of the pyroxenes are expanding too as the result of enhanced solubility of Al components in all pyroxenes and of enhanced solubility of En–Fs components in cpx. An important consequence of the increased solubility of the aluminous components is that the location of the plagioclase + pyroxene thermal divide moves away from the Qtz component with increasing pressure. Thus in Fig. 3b this thermal divide sweeps across the TJ composition between 10 kbar (three-phase triangles point to the left) and 13 kbar (three-phase triangles point to the right); whereas in Fig. 2b the thermal divide has not quite reached the HLCA point at 13 kbar. Also important are the changes in orthopyroxene composition. In Fig. 2a and b the experimental orthopyroxenes at 11·5 kbar overtake the composition of an aluminous *opx* megacryst with 8·4 wt % Al_2O_3 from Harp Lake (Emslie, 1980); similarly, orthopyroxenes produced in the TJ experiments nearly overtake the compositions of the Rogaland megacrysts (Duchesne & Maquil, 1987) by 13 kbar. Finally, the liquidus boundaries involving *plag*, *lpyx*, and high-Ca pyroxene move across the HLCA and TJ bulk compositions in both projections at pressures of 11–13 kbar.

The only significant difference in the phase equilibria between the HLCA and TJ series is in terms of clinopyroxene composition: at 10–13 kbar a low-Ca pigeonite coexists with subcalcic augite and orthopyroxene along the TJ *plag* + *lpyx* + *aug* liquidus boundary (Fig. 3b); whereas a single clinopyroxene with intermediate Wo content coexists with orthopyroxene along the HLCA *plag* + *opx* + *cpx* liquidus boundary (Fig. 2b). This intermediate *cpx* is probably a supercritical clinopyroxene, resulting from the intersection of the crest of the clinopyroxene solvus with the solidus that rapidly terminates all *aug* + *pig* boundary curves at critical end points with increasing pressure (Longhi & Bertka, 1996). Despite the lower *mg*-number the TJ clinopyroxenes are subsolvus because of their lower temperatures (~100°C lower than HLCA), caused in part by lower *mg*-number and in part by the fluxing action of TJ's higher TiO_2, K_2O, and P_2O_5 concentrations.

Finally, despite significant differences in their chemical compositions, HLCA and TJ display remarkably similar liquidus equilibria. It should be noted that at low pressure the bulk compositions project within the *plag* (± *aug*) liquidus field in the [Wo] projections (Figs 2a and 3a) and within the *plag* + *ol* liquidus field in the [Pl,Ilm] projections (Figs 2b and 3b). As pressure increases, not only do the liquidus boundaries shift such that the *plag* + *opx* + *cpx* boundary curve sweeps across each composition in both projections at approximately the same pressure (11–13 kbar), but the *opx* + *cpx* tielines sweep across HLCA and TJ as well. This means that not only are the two bulk compositions multi-saturated in the same pressure range, albeit at different temperatures, but that they also lie in the plagioclase + pyroxene thermal divide. Therefore, neither composition can be derived by fractional crystallization of mantle-derived basaltic magmas; but each can be produced by melting of a (distinct) mafic source.

DISCUSSION

Effects of H_2O on liquidus equilibria

Anorthosites and associated rocks are widely believed to have crystallized from relatively anhydrous magmas (e.g.

Morse, 1982). Evidence is both direct and indirect: amphibole usually appears only as a late-stage replacement mineral; thermometry on ternary feldspars in associated mafic intrusions indicates only modest depression of the dry liquidus (Fuhrman *et al.*, 1988); typically there are no hydrothermal deposits or vein systems; and contact metamorphic aureoles characteristically reach the granulite facies with anhydrous assemblages (e.g. Berg, 1977). Nevertheless, water can have dramatic effects on liquidus equilibria, so it is wise to look for evidence of its effects. A number of recent experimental studies involving melting of mafic materials in the range of 3–7 kbar and $P_{H_2O} < P_{total}$ show that even modest amounts of water (as little as 2 wt % at 5 kbar) produce high-SiO_2 liquids (Baker & Eggler, 1987; Beard & Lofgren, 1991; Springer & Seck, 1997). Conversely, Figs 3b and 4b predict a eutectic-like nature for D and stability of the plagioclase + pyroxene thermal divide at 5 kbar, both of which should inhibit silica enrichment. The Qtz content of point D will increase with decreasing anhydrous pressure, causing D to become an *ol* peritectic and eliminating the plagioclase + pyroxene thermal divide. Thus lower pressures of crystallization should enhance the potential for silica enrichment in evolved liquids. Increasing H_2O content in *liq* at constant pressure has a similar effect, so lack of silica enrichment at 3 or 4 kbar places even stronger restrictions on the permissible amount of dissolved water. As will be discussed shortly, limited silica enrichment is observed in several massifs that crystallized at $P \leq 5$ kbar; and in those cases where extensive fractional crystallization does lead to silica saturation, the paucity of amphibole in evolved rocks attests to relatively low H_2O in the parental liquids. Thus there is little evidence of water exerting an important control on crystallization processes.

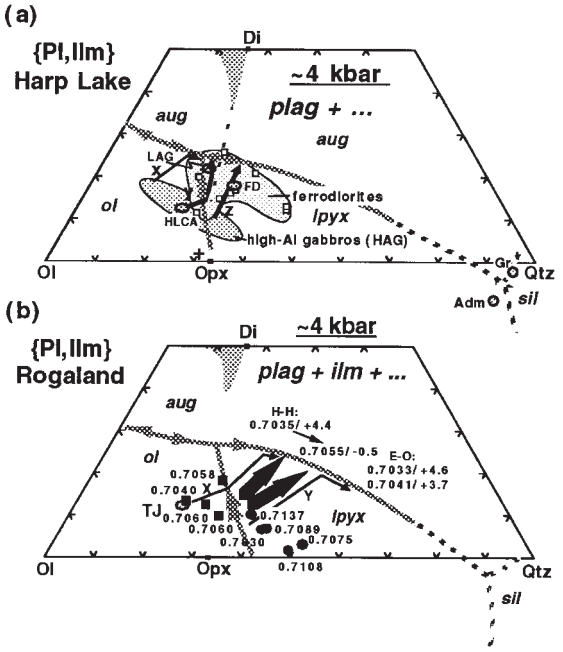

Fig. 4. Crystallization paths of anorthositic and mafic magmas at (a) Harp Lake and (b) Rogaland. Projection schemes as in Fig. 1b. (a) LAG, average low-Al gabbro; FD, average ferrodiorite; Gr, average granite; Adm, average adamellite; □, ferrodiorite compositions projected from Pl, Ilm, Apa and Mgt components. All rock data from Emslie (1980). Heavy cross is 5 kbar experimental *opx* as in Fig. 2. Paths x, y and z show range of mafic crystallization sequences; y and z also show two major low-pressure anorthosite crystallization paths. (b) ■, Bjerkreim–Sokndal (Bk–Sk) and Hidra chill margins from Duchesne *et al.* (1989); ●, Bk–Sk chill margins from Wilson *et al.* (1992); adjacent numbers are initial $^{87}Sr/^{86}Sr$ ratios (Demaiffe *et al.*, 1986; Robins *et al.*, 1997). Large arrows are anorthosite crystallization paths at low pressure; adjacent numbers are initial $^{87}Sr/^{86}Sr$ ratios and ε_{Nd} (Demaiffe *et al.*, 1986; Menuge, 1988); small arrows are mafic fractional crystallization paths. E-O: Egersund–Ogna body; H-H: Haland–Helleren body.

Megacrysts and their parent magmas

The close correspondence of 10–13 kbar experimental orthopyroxene compositions and those of highly aluminous (7–9 wt % Al_2O_3) *opx* megacrysts (HAOM) in Figs 2 and 3 is good evidence for a high-pressure (10–13 kbar) origin for these large crystals. At the same time, various geobarometric techniques have yielded much lower pressures, i.e. 3–5 kbar (Ashwal, 1993), for the crystallization of the anorthositic massifs, thus forming the basis for polybaric models in which the megacrysts are rafted by plagioclase-rich suspensions from the depths where they formed to magma chambers in the upper crust (e.g. Duchesne, 1984; Emslie, 1985). Yet, many megacrysts have Al_2O_3 concentrations in the range of 4–6 wt % and it is not clear whether these compositions represent primary crystallization or re-equilibration. In Fig. 3, which is based on experiments from one composition (TJ), *opx* compositions show a progressive increase in Mg-Ts component (hence Al_2O_3) with increasing pressure, and *opx* from the TJ experiments just reaches the range of Rogaland HAOM compositions at 13 kbar. In Figs 1b and 2b, however, it is clear that *opx* coexisting with *plag*, *cpx*, and *liq* has a range of Mg-Ts contents at constant pressure depending on liquid composition. Thus *opx* coexisting with *liq* at the low-Qtz end of the *opx* + *aug*/*cpx* + *plag* boundary curve (D → B → B′) reaches the field of HAOM compositions by 6 kbar (Fig. 2) and moves past the HAOM field by 13 kbar; whereas *opx* coexisting with liquids close to the plagioclase + pyroxene thermal divide (C) has lower Mg-Ts contents and reaches only the center of the HAOM field by 13 kbar. Predictably, *opx* coexisting with *liq* on the *opx* + *aug*/*cpx* + *plag* boundary curve at silica saturation will have still lower Mg-Ts contents. Thus there is an intrinsic

uncertainty in estimating pressure from HAOM compositions alone, whether the means be graphical or by algorithm (e.g. Emslie *et al.*, 1994), and the best one can do is to estimate a minimum pressure, i.e. the pressure at which the composition of the most aluminous *opx* sweeps across the HAOM composition of interest. The range of minimum pressures for the HAOM compositions plotted in Fig. 2b is thus ~6 kbar for the least aluminous HOAM to ~10 kbar for the most aluminous (8·3 wt % Al_2O_3) HAOM.

The one exception to this large uncertainty is a case where the liquid composition is known. Wiebe (1985, 1986) described nepheline-normative Proterozoic dikes from Nain containing HAOM as separate, anhedral crystals and as parts of nodules intergrown with *plag*. One of these HAOM compositions with $Al_2O_3 = 6{\cdot}2$ wt % and *mg*-number = 0·74 (shaded diamond) and its host dike composition (asterisk) are illustrated in Fig. 2. Wiebe (1986) argued that comparison of Cr and incompatible element abundances in the HAOM and the dike matrices indicates that the HAOM crystallized from more primitive liquids. This argument is consistent with the projections which indicate that at no pressure is the liquid composition close to *opx* saturation. However, at pressures ≥ 6 kbar this liquid could easily have fractionated from liquids that had reacted *opx* out at D or B or B′ depending on the pressure. If the parental liquids of the HAOM were less differentiated relatives of the host dikes, then it is reasonable to assume that HAOM crystallized from a liquid close to the low-Qtz end of the *opx* + *aug*/*cpx* + *plag* liquidus boundary. In this case the true pressure estimate would be equivalent to the maximum pressure estimate. At 6 kbar the most aluminous experimental *opx* has not yet reached the HAOM composition, whereas at 10 kbar the most aluminous *opx* is well past the HAOM composition. This progression yields an estimate of 8 ± 1 kbar for the minimum crystallization pressure, which in this case is possibly the actual pressure.

Crystallization of anorthositic and related magmas at Harp Lake and Rogaland

There is little direct evidence of crystallization pressure in anorthositic rocks themselves; however, application of various geobarometers to mineral assemblages in contact metamorphosed country rocks (e.g. Berg, 1977; Jansen *et al.*, 1985) and in associated mafic intrusions (e.g. Kolker & Lindsley, 1989; Vander Auwera & Longhi, 1994) in most cases yields pressures in the range of 3–5 kbar. There is now emerging a combination of field and geochemical evidence that various Fe-rich dioritic to monzonitic bodies ranging in size from small lenses to small layered intrusions formed by segregation of liquids residual to the crystallization of the anorthosites (e.g. Owens *et al.*, 1993; Mitchell *et al.*, 1996). The crystallization paths of these intrusions combined with the pressure constraints provide important limits on the compositions of the liquids in the later stages of anorthosite crystallization. Other, evolved intrusive bodies, e.g. the Rogaland dikes (Duchesne *et al.*, 1989), have been shown to be plausible differentiates of more primitive mafic bodies intruded at the same level as the anorthosites (Vander Auwera *et al.*, 1998). These primitive mafic bodies not only have the same minerals as the anorthosites, but overlapping mineral compositions and in some cases similar crystallization patterns. Examples of such bodies include the Maloin Ranch and Greaser plutons in the Laramie Complex of Wyoming (Kolker & Lindsley, 1989; Mitchell *et al.*, 1996) and the Hidra and Bjerkreim–Sokndal bodies in Rogaland, Norway (Demaiffe & Hertogen, 1981; Duchesne, 1987; Wilson *et al.*, 1996). It must be emphasized, however, that massif anorthosites are complex, composite intrusions typically involving several parental liquids, so individual mafic bodies may not display the crystallization patterns seen in the associated anorthosites.

Figure 4 is an attempt to portray the crystallization patterns of both the mafic rocks and anorthosites from the Harp Lake and Rogaland massifs at the final level of emplacement. In each case a set of 4 kbar liquidus boundaries has been interpolated from the diagrams in Figs 2b and 3b. For the HLCA series (Fig. 4a) the liquidus boundaries are drawn such that the *ol* + *lpyx* + *aug* + *plag* + *liq* pseudo-invariant point (D) is a eutectic, whereas the *ol* + *lpyx* + *plag* + *liq* boundary is a reaction curve with *ol* reacting with *liq*. The *ol* + *lpyx* + *plag* + *liq* boundary curve crosses the plagioclase + pyroxene thermal divide (dotted line in Fig. 4a). Thus there are some high-Al gabbroic liquids with relatively low Wo components that may cross the trace of the divide in the *ol* + *plag* field and subsequently crystallize *lpyx* + *plag* ± *aug* en route to eventual saturation with a silica phase, even in the absence of water. Liquids with higher Wo, which reach the *ol* + *lpyx* + *plag* + *liq* boundary curve on the low-silica side of the thermal divide may still react *ol* out in favor of *lpyx*. However, progress toward silica saturation is thwarted by the plagioclase + pyroxene thermal divide, which forces such liquids to crystallize *aug* after *opx* and then reprecipitate *ol* at the eutectic D. In Fig. 4b the effects of higher concentrations of alkalis in the TJ series overwhelm the effects of lower *mg*-number and shift the *ol* + *lpyx* + *plag* + *liq* boundary curve entirely to the high-Qtz side of the pyroxene join rendering the thermal divide metastable and constraining pseudo-invariant point D to be an *ol* peritectic.

Harp Lake

Figure 4a shows some of the compositional relations at Harp Lake. Emslie (1980) reported that the bulk of

the plagioclase-rich rocks are either plagioclase + olivine cumulates, in which orthopyroxene commonly rims olivine, or plagioclase cumulates with interstitial orthopyroxene; orthopyroxene + plagioclase cumulates are present, but rare; and plagioclase + augite cumulates have not been observed. These features indicate magmas that project either in the *ol* + *plag* or the *lpyx* + *plag* liquidus fields. These features also require that *ol* reacts along the *ol* + *lpyx* + *plag* + *liq* boundary curve. However, the textures of the noritic anorthosites suggest that plagioclase was the sole liquidus phase, so that the parental liquid did not acquire its high Qtz component by differentiation of a troctolitic liquid near the level of emplacement. The presence of the plagioclase + pyroxene thermal divide is problematical because Emslie (1980) did not describe the reappearance of *ol* as a residual phase in leuconoritic rocks, whereas he did note minor quartz in the matrices of some gabbroic rocks. Emslie (1980) suggested that high-Al gabbroic (more properly 'gabbronoritic' or 'noritic') magmas (HAG) similar in composition to HLCA (Fig. 4a), were parental to the anorthositic rocks and the low-Al gabbros (LAG). As described above, with the *ol* + *lpyx* + *plag* boundary curve crossing the trace of the pyroxene join as is in Fig. 4, HLCA can satisfy the crystallization paths of the troctolitic anorthositic magmas (y) and fractionate to low-Al gabbro as well because of the influence of the plagioclase + pyroxene thermal divide; whereas a slightly more Qtz-rich composition can yield the noritic anorthosites (z). No equivalent to path x (troctolite → olivine gabbro) has been reported among the anorthosites.

Even more evolved than the low-Al gabbros are the ferrodiorites, which contain abundant oxides and apatite. Although Emslie (1980) did not identify the various opaque minerals, similar rocks in other localities typically contain a titanomagnetite as well as ilmenite (Vander Auwera *et al.*, 1998). Therefore, we have projected these compositions from apatite and magnetite components, as well as plagioclase and ilmenite, to minimize the effects of accumulation of these phases. As a result of a different projection scheme plus lower *mg*-number, the liquidus boundaries drawn in Fig. 4a are not appropriate to the ferrodiorites; however, the position of the thermal divide remains relevant. The compositions of the ferrodiorites occupy an irregular-shaped area with two lobes: one sits astride the plagioclase + pyroxene thermal divide; the other prominent lobe extends toward granitoid compositions. This second lobe is presumably the locus of the *lpyx* + *aug* + *plag* liquidus boundary for these compositions. It is thus possible that there are at least two types of ferrodiorite: one derived from liquids close to the LAG composition that were prevented from evolving toward Qtz by the thermal divide; the other from liquids on the high-Qtz side of the thermal divide. In the latter case, the parental liquids may have derived from a troctolitic parent with low-Wo (dashed portions of the z trend), or from a parent similar to HLCA but with higher H_2O content, or from a primary liquid with intermediate composition (solid portion of the z trend).

Finally, the field of the ferrodiorites stops far short of the compositions of the average adamellite (Adm) and granite (Gr) in Fig. 4a, which have far more extensive outcrops than any of the mafic rocks (Emslie, 1980). The gap in composition between the ferrodiorites and granitic rocks [discussed in some detail for the Nain Province by Emslie *et al.* (1994)] is readily explicable if the plagioclase + pyroxene thermal divide is stable: most liquids derivative to the high-Al gabbros will either be trapped on the low-Qtz side of the divide or 'perched' in the divide itself; even liquids with sufficiently low Wo or high H_2O to breach the divide in the *ol* + *plag* field will none the less require relatively large amounts of crystallization to reach silica saturation because of the orientation of the *opx–liq* tieline and the small compositional contrast between crystals and liquid when orthopyroxene begins to crystallize. In addition to the difficulty in producing granitic liquids by fractional crystallization of anhydrous mafic magmas, there is also the fact that the volume of granitoids at Harp Lake is much greater than that of the mafic rocks. Both observations are consistent with the arguments made by Emslie *et al.* (1994) that the Nain granitoids were produced by distinct episodes of crustal melting.

Our analysis lends further support to the proposals by Emslie (1980) and Fram & Longhi (1992) that a high-Al gabbro composition was parental to Harp Lake, but we do not imply that any single pulse of magma or even single composition generated all of the anorthositic rocks, gabbros, and ferrodiorites. High-Al gabbros formed from magmas that reached the intrusion level as mostly liquid, whereas the leucocratic rocks formed from magmas that intruded with as much as 70% plagioclase suspended in at least two different high-Al gabbroic liquids (Longhi *et al.*, 1993); and ferrodiorites may have formed as derivatives of either the anorthositic or gabbroic magmas.

Rogaland

The situation in Rogaland is somewhat different from that at Harp Lake. There are three distinct, apparently diapiric anorthositic massifs [Egersund–Ogna (E–O), Haland–Heleren (H–H), Åna–Sira (A-S)] plus a large layered mafic intrusion [Bjerkreim–Sokndal (Bk-Sk)] (Duchesne & Michot, 1987). The anorthositic rocks appear more uniform mineralogically than at Harp Lake—plagioclase and orthopyroxene in varying sizes, shapes, and proportions being dominant with minor oxides only in H–H and A–S—but in the Egersund–Ogna massif there is a cryptic geographical variation in plagioclase composition. Plagioclase crystals from the center of this massif have

compositions that cluster independent of size or texture in the range of $An_{45–55}$ with Sr concentrations in the range of 800–1100 ppm. There are two typical crystallization sequences at the level of emplacement of the three massifs, represented in part by the large arrows in Fig. 4b: one is *plag*, *plag* + *opx*, *plag* + *opx* + *ilm* with augite apparently absent (E–O); the other is *plag*, *plag* + *ilm*, *plag* + *pig* + *ilm* (H–H, A–S). A sequence similar to (H–H, A–S) with augite appearing late (path y) is observed in the lower macrocyclical units of the adjacent Bk–Sk layered intrusion (Wilson *et al.*, 1996). The upper Bk–Sk macrocyclical units (III, IV) display a crystallization sequence similar to that illustrated for the TJ composition in Fig. 4b (path x), in which olivine reacts to form orthopyroxene and ilmenite with augite appearing late. Previously, Vander Auwera & Longhi (1994) showed that TJ was similar to, but slightly less primitive than the magma parental to the upper Bk–Sk macrocycles. A comparison between phases from the high-pressure experiments on TJ and the E–O megacrysts suggests that a liquid generally similar to TJ was parental to the E–O anorthosites. At 13 kbar, where TJ is cosaturated with *opx* and *plag*, the liquidus *opx* contains 7·1% Al_2O_3 and 410 ppm Cr with *mg*-number = 0·69, and the coexisting *plag* is An_{44} and contains 1140 ppm Sr (Vander Auwera *et al.*, 1993). Both *opx* and *plag* compositions are similar to, but less primitive than typical megacrysts (*opx*: 7–9% Al_2O_3, 600–900 ppm Cr, *mg*-number = 0·77–0·59; *plag:* $An_{45–55}$, 800–1100 ppm Sr) from the center of the E–O massif (Duchesne & Maquil, 1987). Although Cr in the high-pressure *opx* falls well below the range of Cr in the megacrysts, it should be noted that the TJ Cr concentration lies in the center of a range in Cr concentrations from the various Bk–Sk chill margin samples that varies by a factor of four (Duchesne *et al.*, 1989; Robins *et al.*, 1997), so postulating a jotunitic magma with Cr content greater than TJ is certainly plausible. Furthermore, the compositions of plagioclase from the central portion of the E–O massif overlap those from Bk–Sk in terms of Na, K, Ba, and Sr, yet are distinct from those of modern basalts as well as those from Precambrian layered intrusions such as the Bushveld and Stillwater (Duchesne & Demaiffe, 1978; Emslie, 1985). So it is reasonable to conclude that jotunitic magmas, similar to TJ, but with higher *mg*-number and Cr, were parental not only to the Bk–Sk intrusion (path x in Fig. 4b) but also to the *opx* megacrysts and much of the plagioclase in the central portion of the E–O massif. As more data come available, it may turn out that TJ and the parental liquid of the upper Bk–Sk macrocyclical units were more similar to the H–H and A–S parental liquids, whereas the parental liquids of the lower Bk–Sk macrocyclical units were more similar to the central E–O parent liquid. The absence of primary olivine in the anorthosite massifs and the initiation of the noritic (lower) Bk–Sk macrocycles by plagioclase accumulation (pC) argue for parental liquids, saturated only in plagioclase, that acquired their relatively high Qtz components below the level of emplacement (y in Fig. 4b). Thus in Rogaland there were both troctolitic and noritic parental liquids, and all of these liquids were jotunitic, but only the noritic liquids produced anorthositic intrusions.

Initial $^{87}Sr/^{86}Sr$-isotope ratios (I_{Sr}) and ε_{Nd} are shown for the E–O *opx* and *plag* megacrysts (0·7033/ + 4·6, 0·7041/ + 3·7; Demaiffe *et al.*, 1986) and H–H anorthosites (0·7035/ + 4·4, 0·7055/ + 0·5; Menuge, 1988) are shown in Fig. 4b, as are I_{Sr} ratios for various chill margins of associated mafic intrusions (squares and circles) As in other complexes, the megacrysts have the most isotopically primitive compositions (e.g. Ashwal, 1993) and there is an obvious correlation of weakly increasing I_{Sr} with more strongly decreasing ε_{Nd} among the anorthosites, which is generally agreed to be the result of crustal contamination following accumulation of *plag* with high Sr and low Nd concentrations. Given the size of the massifs and their intrusion as heavily crystalline masses (Duchesne, 1984), most of the contamination must have occurred before emplacement. Among the Bk–Sk chill margin samples (filled circles; Robins *et al.*, 1997) I_{Sr} generally increases as Qtz content increases and Wo decreases, which is consistent with progressive high-level granitic–gneissic contamination of the Bk–Sk parent magmas. Wilson *et al.* (1996) have also documented progressive Sr-isotopic contamination within the Bk–Sk intrusion (0·7049–0·7085). There are no Nd-isotopic data available for Bk–Sk, but ε_{Nd} varies from 0·3 to –2·7 in the chill margin samples (the five circles with the highest Qtz component in Fig. 4b) reported by Robins *et al.* (1997) with no apparent covariation with I_{Sr}. The most significant features of these data are that (a) the most isotopically primitive anorthosites have compositions overlapping those of both the plagioclase and orthopyroxene megacrysts, and (b) the most isotopically primitive Bk–Sk chill margin composition ($I^{87}Sr/^{86}Sr$ = 0·7040) is in the range of the megacrysts and most primitive anorthosites. Given the likelihood that the megacrysts reflect high-pressure processes, the anorthosite and Bk–Sk parental liquids thus reached relatively high Qtz and low Wo contents at high pressures, enabling them to crystallize *opx* at lower pressures without extensive assimilation of a granitic component.

Survey of anorthositic and related magmas

From the previous discussions it should be clear that despite large differences in isotopic composition and even some significant differences in minor element concentrations (Ti, K, P) the overall petrological characters

of the magmas parental to the Harp Lake and Rogaland massif anorthosites are similar: the troctolitic–noritic and noritic mineralogies require liquid compositions with relatively low Wo and moderate Qtz contents. In Fig. 5 we explore the relation between composition and phase equilibria for a wider range of complexes. Figure 5a, which emphasizes crystallization at the level of emplacement, depicts crystallization paths from various anorthositic massifs as large arrows. Pointed tips show the direction of further crystallization; blunt tips indicate magmas in thermal divides. Also shown are the compositions of some potentially parental mafic rocks. Two features are important. First, the crystallization paths of many of the anorthosites are consistent either with parental liquids (i.e. the beginnings of the arrows) that project near HLCA and TJ in the high-pressure locus of the plagioclase + pyroxene thermal divide or with more noritic compositions that project to the high-Qtz side of the divide. This feature, along with the presence of the highly aluminous *opx*-megacrysts, which ties the anorthosite parent magma to an episode of high-pressure crystallization, prohibits derivation of the parental magma at depth from an even more primitive liquid with significantly lower Qtz content. The second feature is the wide array of mafic compositions (tick marks show the displacement of the projection points caused by removal of 10% of the Fe as ferric), some of which are obviously not parental to the bulk of the associated anorthosites. Perhaps the best example is the Kiglapait intrusion (*Kg*) in the Nain province of Labrador, which has extensive accumulations of troctolite overlain by olivine gabbro that contains no primary low-Ca pyroxene (Morse, 1979). The parental liquids to such sequences of cumulates should logically project well within the *ol* + *plag* liquidus field on a line between the Ol component and the thermal maximum on the *ol* + *plag* + *aug* liquidus boundary (compare the blunt-ended arrow in Fig. 5a); and, indeed the chill margin composition of Nolan & Morse (1986) does plot close to this thermal divide. However, no anorthosites with comparable mineral parageneses have been reported in the Nain region (e.g. Ranson, 1981; Xue & Morse, 1993). Interestingly, though, the Kiglapait crystallization sequence is similar to that described in the central dome of the Laramie Complex (LaC) by Frost *et al.* (1993).

Some of the fine-grained high-Al gabbroic dike compositions from the Greaser (and Strong Creek) intrusions at Laramie (Mitchell *et al.*, 1995) also project close to the olivine + augite + plagioclase thermal divide, as do dikes from the Newark Island intrusion (Wiebe & Snyder, 1993), and the Hettasch chill margin (Berg, 1980), although crystal accumulation may have compromised these compositions somewhat.

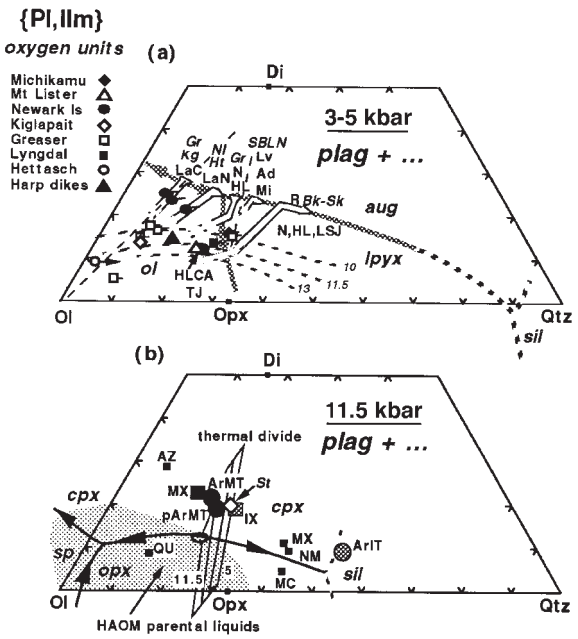

Fig. 5. Comparison of rock, parental magma and potential source compositions. (a) Schematic plagioclase liquidus surface at 3–5 kbar. Open arrows indicate inferred crystallization paths; blunt ends indicate magma perched in or trapped by a thermal divide; dotted portions of the arrows indicate greater ranges of composition for some of the listed localities. Abbreviations (italics, mafic intrusion; plain text, anorthosite): *Kg*, Kiglapait; *Gr*, Greaser; *Nl*, Newark Island; *Ht*, Hettasch; *SBLN*, Slam Bang Leuconorite; *Bk-Sk*, Bjerkreim–Sokndal; LaC, Laramie central dome; LaN, Laramie northern dome; N, Nain; HL, Harp Lake; Lv, Labrieville; Ad, Adirondacks; Mi, Michikamau; R, Rogaland; LSJ, Lac St Jean. Short lines attached to symbols show the effect of removing 10% of the total Fe as ferric. Dashed curves are the traces of the *lpyx* + *aug* + *plag* cotectics at 10, 11·5 and 13 kbar from Fig. 2b. Sources of data: Michikamau, Emslie (1970); Mt Lister dikes, Emslie *et al.* (1994); Newark Island intrusion, Wiebe & Snyder (1993); Kiglapait, Nolan & Morse (1986); Greaser dikes, Mitchell *et al.* (1995); Lyngdal hyperites, gabbronorites, Demaiffe *et al.* (1990); Hettasch, Berg (1980); Harp dikes, Meyers & Emslie (1977). (b) Plagioclase liquidus surface at 11·5 kbar from Fig. 2b; thermal divide is constructed from *opx* + *aug* tielines from 5 to 11·5 kbar. Large filled symbols from Rudnick & Fountain (1995) table 6: MX, mafic xenoliths; ArMT, Archean mafic terranes; pArMT, post Archean mafic terranes; IX, intermediate xenoliths; ArIT, Archean intermediate terranes. Small filled squares, average feldspathic granulitic xenoliths from Emslie *et al.* (1994) table 6: AZ, Arizona; QU, Queensland; MX, Mexico; NM, New Mexico; MC, Massif Central; ◇, *St.* is bulk composition of the Stillwater Banded Zone, Hess (1960). Shaded area, constructed from Fig. 2b, shows plagioclase-saturated liquids that may coexist with *opx* containing ≥8 wt % Al_2O_3.

Greaser (Laramie)

There are several compositions involved in the Greaser intrusion. Frost *et al.* (1993) described layers of olivine gabbronorite, gabbronorite, and ferrogabbro, but no troctolite in the Greaser intrusion. This description is generally consistent only with the Greaser dike composition (open box) that projects close to the *ol* + *lpyx* + *plag* liquidus boundary (the reappearance of

Fe-rich olivine without quartz in the residua of some ferrogabbros is an indication that after reacting out olivine the liquid was blocked from silica enrichment by the plagioclase + pyroxene thermal divide). The Greaser composition with very high Ol content probably reflects olivine accumulation, but the cluster of three dike compositions close to Kiglapait chill margin are probably very similar to the liquids parental to the anorthosites of the central dome described above.

Newark Island (Nain)

The three Newark Island dike compositions are from rocks that contain hornblende and biotite, but no olivine, despite their being obviously olivine-normative (Wiebe & Snyder, 1993). None the less, the compositions are generally consistent with the cumulate sequence of troctolite followed by olivine gabbro with minor late-stage gabbronorite, as suggested by the open arrow. However, the stratigraphic sections presented by Wiebe (1983, 1988) suggest 30–40% troctolite crystallization rather than the ~20% predicted from the projection points in Fig. 5a, thus supporting the existence of a parent magma with even lower Wo than the dikes.

Hettasch (Nain)

The Hettasch chill margin composition (Berg, 1980) apparently reflects olivine (+ plagioclase) accumulation (supported by comparison of most magnesian olivine in the intrusion Fo_{73} with a calculated Fo_{82} liquidus olivine for the composition). The proximity of the Hettasch point (O) to the Ol component makes its predicted crystallization sequence especially sensitive to small analytical errors or non-isochemical alteration. Berg (1980) described a thick cumulus sequence of troctolite overlain by gabbronorite, which suggests a parental liquid projecting approximately on a line between Ol and the pseudo-invariant point—this requires a small displacement of the composition toward the Qtz component. As removal of about 50% troctolite component is needed to make the liquidus olivine of the chill margin composition equivalent to those observed in the intrusion, the Hettasch parent liquid (tip of the small arrow) should project approximately in the center of the *ol* + *plag* liquidus field, close to and to the right of the Kiglapait chill composition.

Although neither the Newark Island nor the Hettasch crystallization sequence is prominent among the anorthositic rocks of Nain (Morse, 1982), the major sequence in anorthositic rocks of the northern dome (LaN) at Laramie (Frost *et al.*, 1993), where *ol* + *plag* accumulation gives way to *ol* + *plag* + *aug* + *lpyx*, is similar to that of the Hettasch, whereas the Newark Island sequence is apparently transitional between those of the northern and central domes at Laramie. Thus, although the predominant parental magma of massif anorthosites appears to be troctolitic–noritic, it is evident that troctolitic–gabbroic magmas with lower Qtz contents also formed anorthosite massifs. What all these magmas seem to have in common is low Wo content, which leads to extensive intervals of *ol* + *plag* crystallization in liquids with low to intermediate Qtz and extensive *lpyx* + *plag* crystallization in liquids with higher Qtz, but only in the Laramie Complex have the magmas with lower Qtz contents formed major anorthositic units. Thus the liquids that formed the more primitive mafic intrusions have much the same range in composition and crystallization order as the liquids entrained in suspensions that formed the anorthositic rocks. Not surprisingly, both groups of liquids have similar lines of descent (Vander Auwera *et al.*, 1998) and determining the parentage of highly evolved rocks within the complexes may accordingly be difficult.

Isotopes

Although the Harp Lake and Rogaland massifs do not encompass the full range of petrological and structural variation in Proterozoic anorthosites, they none the less span a sufficiently wide range of variation that both common ground and differences are likely to be characteristic of the group. For example, most massif anorthosites are either noritic or troctolitic–noritic (Ashwal, 1993)—Laramie, where augite is the dominant mafic mineral (Frost *et al.*, 1993), is a notable exception. Also, differences in the range of ε_{Nd} correlate with basement. For example, $\varepsilon_{Nd} = -3$ to -6 in anorthosites at Harp Lake, which is situated in Archean terrane, whereas $\varepsilon_{Nd} = 0$ to $+5$ in Rogaland, which is situated in Proterozoic terrane (Demaiffe *et al.*, 1986). This correlation of ε_{Nd} with basement is characteristic not only of the massifs as a group (Ashwal & Wooden, 1983), but also of individual provinces where anorthositic intrusions span major tectonic boundaries (e.g. Nain, Emslie *et al.*, 1994; Laramie, Mitchell *et al.*, 1995). Within complexes megacrysts of pyroxene and plagioclase tend to have among the lowest I_{Sr} ratios and highest ε_{Nd} values (Demaiffe *et al.*, 1986; Ashwal, 1993; Scoates & Frost, 1996). There also appears to be a widespread pattern of ε_{Nd} being typically higher and I_{Sr} being lower in troctolitic anorthosites than in associated noritic anorthosites (Ashwal, 1993; Wiebe, 1994). Where there are extensive data available (e.g. Nain, Emslie *et al.*, 1994; Laramie, Scoates & Frost, 1996) there is an overall negative correlation of I_{Sr} and ε_{Nd}, indicating a mixing process between a local basement component (high I_{Sr} and low ε_{Nd}) and another more primitive component. Scoates & Frost (1996) showed that the entire range in Nd and Sr isotopic composition at Laramie can be accounted for by mixing only 10% Archean basement with the most isotopically

primitive high-Al gabbro. Similarly, it can also be shown that the entire Nd isotopic range in Nain can be accounted for by mixing $\leq 20\%$ Archean basement with the most primitive mafic composition listed by Emslie *et al.* (1994). Even the most extreme examples of a primitive component, however, fall short of unambiguous depleted mantle values ($I_{Sr} < 0{\cdot}7030$, $\varepsilon_{Nd} > +5{\cdot}5$ at ~1 Ga). Emslie *et al.* (1994) suggested that the primitive component is enriched mantle; but crustal components can satisfy the constraints equally well (Demaiffe *et al.*, 1986; Owens *et al.*, 1994).

There are numerous examples of conflicting major element and isotopic trends that collectively suggest that most of the isotopic mixing occurs at depth. For example, at Laramie there are examples of apparently local progressive contamination of individual anorthosite intrusions (e.g. Poe Mountain, Scoates & Frost, 1996), which suggest assimilation following emplacement, but the observed variations form only a small part of the isotopic array for the complex. On the other hand, high-Al gabbros span the entire range of ε_{Nd} at Laramie with little change in major element composition (Mitchell *et al.*, 1995); whereas among the anorthosites the highest normative An contents (50–55) are observed with both the lowest (0·7042—Poe Mountain) and the highest (0·7055—Snow Creek) I_{Sr} ratios (Scoates & Frost, 1996). Similarly, Owens *et al.* (1994) showed a clear positive correlation between I_{Sr} and normative An in anorthosites from Labrieville, St Urbain, and Morin. These observations suggest that most of the isotopic mixing occurred before emplacement of the anorthositic magmas with only subtle effects on the major element composition of the parent magmas. There are, however, no firm isotopic constraints that distinguish between assimilation at depth by a mantle-derived magma and melting of mixed sources. So other lines of evidence are needed.

High-pressure phase relations

The fact that parental compositions such as HLCA and TJ lie in or near a thermal divide at the pressures where they coexist with two pyroxenes and plagioclase implies not only that their source regions consist of these minerals, but also that the source compositions project in or near this thermal divide. The same constraints do not apply to the low-Qtz mafic liquids that formed the Kiglapait, Hettasch, and Newark Island mafic intrusions, the Greaser dikes, or the Laramie anorthosites. Indeed, considered in isolation such liquids might reasonably be interpreted to be unusual varieties of mantle-derived liquids. None the less, their parental liquid compositions project on or close to the traces of the 10–13 kbar *plag* + *lpyx* + *aug/cpx* liquidus boundaries (Fig. 5a), so these compositions are also consistent with melting of mafic sources—but sources with lower Qtz contents than that of the thermal divide. Probably these lower Qtz contents are produced by some aluminous spinel that formed during subsolidus reaction of olivine and plagioclase and is exhausted during melting. Similarly, noritic parental magmas project on the traces of the 10–13 kbar *plag* + *lpyx* + *aug/cpx* liquidus boundaries on the high-Qtz side of the thermal divide. Such magmas are consistent with melting a *plag* + *lpyx* + *aug/cpx* source that contains a few percent quartz.

Olson & Morse (1990) and Wiebe (1994) have called attention to 'regional Fe–Al magmas' parental to mafic rocks that are probably, but not so obviously, related to associated anorthositic rocks. Our analysis indicates that these magmas form the low-silica end of a spectrum of anhydrous melts of mafic sources at lower-crustal pressures. It is perhaps a matter of chance and geography that in some complexes (e.g. Harp Lake, Rogaland) mafic rocks that crystallized from liquids similar to those parental to the anorthosites are readily apparent; whereas in other complexes (e.g. Nain) they are not. However, even if magmas similar to the parental magmas of the mafic bodies did not form anorthosites in one complex (e.g. Kiglapait, Hettasch, and Newark Island intrusions in Nain), similar Fe–Al magmas did produce anorthosites elsewhere (e.g. Laramie).

Compositions attributable to the lower crust from compilations of xenolith suites (Emslie *et al.*, 1994; Rudnick & Fountain, 1995) and from averages of granulitic terranes of various ages (Rudnick & Fountain, 1995) are shown in Fig. 5b. These compositions reflect mineralogies dominated by pyroxene and plagioclase, so if anhydrous melting of the lower crust at 10–13 kbar (pressures necessary to produce the HAOM) were to take place, we could reasonably expect liquid compositions with relatively low Wo contents but a petrologically significant range of Qtz contents. Because many of the compositions, including estimates of the average composition of the lower crust (ArMT or pArMT in Fig. 5b), actually project in the polybaric trace of the plagioclase + pyroxene thermal divide, there reasonably might be a clustering of liquid compositions near the pyroxene–plagioclase thermal divide. Additionally, various estimates of the trace element composition of the lower crust are consistent with generation of the parent magmas of the massif anorthosites, such as high Sr concentrations and a lack of Eu anomalies (Taylor *et al.*, 1984; Taylor & McLennan, 1985; Owens *et al.*, 1994) in what would otherwise be evolved compositions. Owens *et al.* (1994) also argued that the observed Sr concentrations in Labrieville plagioclase (~2000 ppm) cannot be produced by contaminating a mantle-derived magma with any likely crustal component.

Melting of the lower crust does pose numerous problems, however. In some cases, isotopic compositions of the anorthositic rocks lie close to mantle evolution curves

and thus appear to support a mantle-derived parent magma. However, the constraints may generally be satisfied if the crustal source separated from the mantle no more than a few hundred million years before the melting event (e.g. Demaiffe *et al.*, 1986; Owens *et al.*, 1994). Another problem is *mg*-number: the Archean and post-Archean mafic terrane averages compiled by Rudnick & Fountain (1995) have *mg*-number = 0·54–0·58, whereas HLCA has a bulk *mg*-number = 0·52. Even if the requisite extensive melting were possible, orthopyroxene would not be a residual phase at $P \geq 11{\cdot}5$ kbar under anhydrous conditions because of the high Wo content in these compositions. Sources similar to the average Queensland mafic xenoliths (QU, Emslie *et al.*, 1994) with higher *mg*-number (0·68) and lower Wo are more suitable for HLCA, but obviously are not as widespread. Possibly a small amount of H_2O could lower the solidus sufficiently to increase the width of the *opx* + *cpx* two-phase field so as to allow residual orthopyroxene in more typical lower-crustal compositions. Melting of the lower crust, either by magmatic heating from below or by crustal thickening or by thrusting tongues of lower crust into the mantle (Andersson *et al.*, 1996), is not the only possible scenario, however. Arndt & Goldstein (1989) and Glazner (1994) have pointed out that mafic to ultramafic intrusions in the mid- to upper crust will be gravitationally unstable and will tend to sink into the lower crust or upper mantle, especially if heating lowers the effective viscosity of the crust. In such cases upwelling asthenosphere or large magma bodies ponded in the upper mantle might supply both the conductive heat that causes the mafic–ultramafic masses to sink out of the crust and the local heat of contact melting. Interestingly, the bulk composition of the Stillwater Banded Zone (Hess, 1960) also projects close to the plagioclase + pyroxene thermal divide and has a relatively high *mg*-number (0·73), although a lower Wo content would be preferable. Furthermore, the upper portions of mafic layered intrusions, which contain more sodic plagioclase, more ferroan pyroxene, plus cumulus Fe–Ti oxides and phosphate, are especially attractive sources for jotunitic magmas: the lower *mg*-number plus higher concentrations of K, Ti, and P can lower the solidus sufficiently such that the *opx* + *aug*/*cpx* tielines extend far enough even at 13 kbar (see Fig. 3b) to encompass compositions with Wo contents as high as that of the Stillwater. A third possibility is that of two-stage partial melting in which the first stage of melting removes a silica-saturated melt from an intermediate source leaving a granulitic (*pyx* + *plag*) restite, whose bulk composition necessarily projects in the thermal divide; a second stage of melting at a higher temperature produces a liquid whose composition also plots in or near the thermal divide. Emslie *et al.* (1994) suggested that such restites would be ideal assimilants to impart many of the trace element features of anorthosites onto mantle-derived melts. However, nearly 100% assimilation would be needed to make a composition like HLCA or TJ.

Fractionation paths

Finally, questions about the mechanism of crustal melting and what conditions led similar liquids to accumulate plagioclase in one case but not in another are beyond the scope of this paper. But lest this deferment raises inappropriate doubts, we wish to emphasize that the phase equilibria presented herein are not only consistent with generating the parental magmas of HAOM, anorthosites, and related mafic rocks by melting of a lower-crustal mafic source, but also generally preclude derivation from melts of peridotitic mantle—and not merely at 11·5 kbar as argued above. The polybaric phase equilibria illustrated in Figs 2 and 3 allow us to consider fractionation paths taken by mantle-derived magmas that pond in upper-mantle or lower-crustal chambers, differentiate, and reach plagioclase saturation with intermediate *mg*-number. Figure 6 shows the trace of the pseudo-invariant points involving *plag*, *lpyx*, *ol*, and *aug*/*cpx* (heavy patterned curves) taken from Fig. 2 and illustrates the permissible anhydrous fractionation paths (open arrows) in three different pressure regimes. At $P \leq 4$ kbar (region I) where the pseudo-invariant point (D) is an olivine peritectic, the high-silica portion of the *aug* + *lpyx* + *plag* liquidus boundary is accessible. Between ~4–6 kbar point D is a eutectic (region II), so high-silica liquids are no longer accessible (opposing arrows), at least not to typical basaltic liquids. Above ~6 kbar point D is an *lpyx* peritectic (region III), so typical evolved basalts will react out *lpyx* and move away from the Qtz component. Only at $P \leq 4$ kbar can assimilation of granitic crust coupled with fractionation (AFC; shaded arrow) cause a multiply saturated liquid to depart significantly from its simple fractionation path because at higher pressures the hybrid liquid either cannot escape the eutectic or it follows the cotectics down temperature away from Qtz.

Also illustrated in Fig. 6 are the compositions of average MORB glasses from the Atlantic and the Pacific, a highly differentiated MORB suite from the East Pacific Rise (filled squares), and some continental tholeiites (filled circles and stars) with relatively low volatile contents that are widely believed to have evolved in lower-crustal chambers before high-level intrusion or eruption. As expected, the locus of these compositions tracks the regions where *lpyx*, *aug*, and *plag* ± *ol* cocrystallize and misses the compositional range necessary to form HAOM together with the troctolitic–noritic crystallization sequences.

It is possible for primitive mantle melts to access compositions similar to HLCA under special conditions.

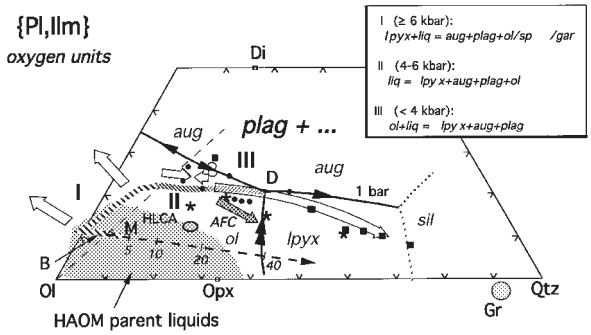

Fig. 6. Fractionation paths of mantle-derived liquids. Heavy dashed curves show the locus of pseudo-invariant points involving *lpyx* from Fig. 2b; pressure increases from right to left. Inset box gives the pressure range for each melting equilibrium. Large arrows show direction of liquid evolution once a fractionating basaltic liquid has reached the pseudo-invariant point appropriate for a given pressure; opposing arrows indicate eutectic relations. Shaded arrow shows assimilation–fractionation (AFC) path for pressure regime III; AFC paths in pressure regimes I and II are similar to simple fractionation paths. Graded line shows wt % mixing of average Harp Lake granite (Gr, Fig. 5a) with liquid at B (Fig. 1). M is representative melt of low-silica mafic source at 10–13 kbar. ■, rocks and glasses from East Pacific Rise (Bender *et al.*, 1986); ○, average Atlantic and Pacific MORB glasses (BSVP, 1981); ●, continental flood basalts: average Askja Myvattn qtz tholeiite, Iceland, average Siberian traps, average upper and lower Deccan flows (BVSP, 1981), average Picture Gorge basalt, average Yakima basalt, average Karoo diabase, average Palisades diabase (Carmichael, 1974). *Individual representative analyses of Keweenawan flows (BVSP, 1981).

For example, a melt with composition equal to HLCA + Ol could reach *plag* saturation near the HLCA projection point at $P \leq 4$ kbar (Fig. 2a), but at such pressures this residual composition would contain less Pl component than HLCA and such a scenario would preclude HAOM. Assimilation of a granitic component into a primitive melt with lower Qtz and Wo than HLCA could change the crystallization trajectory such that the AFC path trends across the projected HLCA composition (Fig. 6). If the evolving liquid composition remains on the *ol* + *plag* liquidus surface and decreases in temperature, then the process is limited to pressures where the plagioclase + pyroxene thermal divide is not stable, i.e. $P \leq 4$ kbar, once again precluding the existence of HAOM. At higher pressures where HAOM are stable and mantle-derived liquids are nepheline-normative, the plagioclase + pyroxene thermal divide creates a barrier even to the most favorable conditions of AFC (e.g. Kelemen, 1990), such that assimilation of granitic material will induce crystallization that drives the hybrid liquid away from the divide, increasing its nepheline content.

Perhaps, the most hopeful scenario for assimilation arises when the magma is saturated only with plagioclase. If a fractionating mantle-derived liquid arrived at the *plag* liquidus surface at 11·5 kbar, the closest its composition could be to HLCA or TJ would be B in Figs 2a and 6. If this liquid rose quickly enough to a depth corresponding to 4 kbar, it would be situated entirely within the plagioclase liquidus volume, and, in a [Pl,Ilm] projection, its initial AFC path would appear to be on a direct line toward the assimilant composition (Gr from Fig. 4a in this case). We recall, on the other hand, that noritic anorthosite magmas from Harp Lake and Rogaland intruded saturated only with *plag*. This constraint limits the amount of *plag* crystallization before emplacement, i.e. pressure release from 13 kbar to 4 kbar. The amount of *plag* that will crystallize alone can be estimated to be ≤15 vol. % by applying the lever law to the 11·5 and (interpolated) 4 kbar liquidus boundaries in Fig. 2a. If the ascending magma was a suspension and retained all of its superheat, it could dissolve as much as 4% suspended *plag* (Table 4). Gradations on the mixing path in Fig. 6 show that if all of the heat released from crystallizing this potential plagioclase (15% from expansion of the plagioclase liquidus field, 4% from superheat) went into assimilating a comparable amount of granitic component, it would indeed be possible to move the B composition to the high-Qtz side of HLCA. Because the amount of *plag* crystallized from the superheated liquid is approximately the amount that was melted, ~19% assimilation would produce a net crystallization of ~15% *plag* from composition B, thus allowing the hybrid liquid to remain at least marginally in the *plag* liquidus field.

Although the major elements permit this idealized AFC scenario, other considerations mediate against it. First, mantle-derived magmas could make norites only if they assimilated at least 20% granitic component (Gr). Yet many leuconorites have relatively primitive isotopic ratios that preclude 20% assimilation of granitic material. Second, energy sinks (heating of country rock to its solidus, heating the granitic melt to the temperature of the mafic liquid) are likely to make this process less efficient. Also, survival of HAOM, even in suspensions, is a testament to their host liquids having never become significantly superheated. Finally, because the olivine + augite + plagioclase thermal divide (dashed line in Fig. 6) is stable below ~6 kbar for compositions with intermediate *mg*-number, the liquidus surface must be saddle shaped with respect to temperature in the vicinity of the thermal divide. This saddle shape produces an exception to the observation of Ghiorso & Kelemen (1987) that mixtures of primitive liquids and eutectic liquids inevitably have temperatures above the liquidus of the mixture. The mixing trend beginning at B in Fig. 6 cuts across the trace of the thermal ridge (dashed line in Fig. 6) and, therefore, could proceed only in the unlikely event that the granitic melt was generated and its temperature was raised to nearly that of liquid B without withdrawing any heat from B on a regional scale. This condition applies to almost all possibly mantle-derived liquids derived

*Table 4: Thermal constraints on superheat and melting (*liq = *HT80E-1)*

Terms

ρ (density; g/cm^3), *T* (temperature; K), *P* (pressure; bars), *V* (volume; cm^3)

α_P (isobaric thermal expansion; K^{-1}) $\equiv \left(\frac{1}{V}\right)\left(\frac{dV}{dT}\right)_P$

$\bar{C}_P^{liq}$ (isobaric heat capacity of liquid)

x_i (mole fraction of oxide *i*)

$(dT/dP)_s$ (adiabatic temperature gradient) $= \left(\frac{\alpha_P T}{\rho \bar{C}_P}\right)$ (Ref. 1)

$(dT/dP)^L$ (liquidus slope)

$(dT/dF)_P$ (temperature drop per wt unit of crystallinity)

$(d\rho/dP)^L$ (liquidus density gradient)

Calculations

gram-atomic weight of HT80E-1 = 64·6 g/mol

$(d\rho/dP)^L$ = 0·007 g/cm^3 per kbar (Ref. 2)

$\bar{C}_P^{liq} = \sum_i (x_i \bar{C}_{Pi}^{liq})$ = 940 cm^3 bar/K per mol = 14·6 cm^3 bar/K per g (Ref. 3)

$(dT/dP)^L$ (HLCA, 0–10 kbar) = 4·2 K/kbar (Ref. 4)

$(dT/dF)_P$ (from 500B-30 and -32) = 1·67 K/wt % (Ref. 4)

ΔT^L (11·5–4 kbar) = $(dT/dP)^L(\Delta P)$ = –31.5 K

α_P = 0·000088/K (from liquid density model) (Ref. 5)

ρ^{liq} (HT80E-1, 1 bar) = 2·70 g/cm^3 @ 1265°C (Ref. 5)

ρ^{liq} (HT80E-1, 11·5 kbar) = 2·70 + $(d\rho/dP)^L(\Delta P)$ = 2·78 g/cm^3

$(dT/dP)_s$ = (0·000088 × 1538)/(2·78 × 4·6) = 0·0033 K/bar = 3·3 K/kbar

potential superheat: $\Delta T^S = \Delta T^L - \Delta T^{adiabat}$ = –31·5 – $(dT/dP)_s(\Delta P)$ = –31·5 – (3·3 × –7·5) = –6·8 K

plagioclase remelting potential: $F = \Delta T^S/(dT/dF)_P$ = –4·0 wt %

References: 1, Stacey (1969); 2, Agee & Walker (1989); 3, Stebbins *et al.* (1984); 4, Fram & Longhi (1992); 5, Bottinga & Weill (1970).

throughout region I. The only exceptions are those that lie along the short portion of region I that extends to the high-Qtz side of the thermal divide. Region I terminates because the increasing pressure stabilizes a garnet-bearing assemblage ($P \geq 13$ kbar)—a condition that appears to be excluded by REE modeling (Simmons & Hanson, 1978). Thus there is a narrow range of possibly mantle-derived liquids projecting near the terminus of Region I (and thus representing fractionation only in the range of 13 kbar > P > 11·5 kbar) that could assimilate granite during ascent through the crust and transform into noritic liquids saturated only with *plag*. As illustrated in Fig. 6, a minimum of ~20% granite assimilation would be required to produce noritic liquids by this mechanism. However, the primitive isotope compositions of some noritic anorthosites do not permit such extensive assimilation. Furthermore, Duchesne & Michot (1987) described the Rogaland massifs as being composed nearly entirely of noritic anorthosites and leuconorites with no mention of troctolitic rocks. It is difficult to envision how 20% granite component could become so uniformly mixed throughout such large volumes of suspension so as to not leave patches of troctolitic anorthosite where only 5 or 10% granite was mixed in.

More silicic troctolitic melts (e.g. M) produced on the *opx* + *cpx* + *plag* liquidus boundary on the low-Qtz side of the plagioclase + pyroxene thermal divide at pressures of 10–13 kbar would be able to intrude upward, assimilate granitic material, remain saturated in only plagioclase, and appear to evolve along a mixing line toward granite, as described above. The same cautions against copious assimilation apply here, too, but as M begins with a higher Qtz component than B, less assimilation is required to move the hybrid composition to noritic compositions. Of course, even less assimilation is needed if the starting point is HLCA. In this way it may be possible to transform crustally derived troctolitic magmas into noritic magmas saturated only in *plag* with a relatively small amount of assimilation of granitic material. Indeed, only a few percent granite assimilation is needed to account for the observation that ε_{Nd} is typically lower and $I^{87}Sr/^{86}Sr$ is higher in noritic anorthosites than in associated troctolitic anorthosites (Ashwal, 1993; Wiebe, 1994).

CONCLUSIONS

Massif anorthosites and their associated mafic rocks crystallized from liquids with low Wo contents and

intermediate *mg*-number. These liquids span a considerable range in Qtz content from nearly nepheline-normative compositions that crystallize troctolitic (ol + plag) and gabbroic (ol + aug + plag) assemblages with no low-Ca pyroxene (e.g. the central dome at Laramie and the Kiglapait intrusion in Nain) to quartz-normative compositions that crystallize noritic assemblages (opx + plag ± ilm) followed by augite-bearing assemblages (e.g. portions of Harp Lake and Nain in Labrador plus Egersund–Ogna, and Bjerkreim–Sokndal in Norway). We have shown here that two compositions that had previously been shown to be suitable parental liquids—HLCA for the Harp Lake anorthosites (Fram & Longhi, 1992) and TJ for the Bk–Sk intrusion (Vander Auwera & Longhi, 1994)—are simultaneously saturated with HAOM-like orthopyroxene, clinopyroxene, and intermediate plagioclase on their respective liquidi at 10–13 kbar and also lie in the plagioclase + pyroxene thermal divide. Despite multisaturation, these compositions cannot be residual liquids to any more primitive liquid derived by melting peridotitic mantle. Such compositions must be melts of pyroxene + plagioclase sources whose compositions already lie in the thermal divide. Although these constraints do not apply to the entire range of liquids parental to the anorthosites, the compositions of these liquids are none the less consistent with partial melting of heterogeneous mafic source regions in the range of 10–13 kbar. The ideal source for HLCA-like liquid is apparently more magnesian than averages of mafic terranes, which are thought to be representative of the lower continental crust (e.g. Rudnick & Fountain, 1995). Other potential sources include restite left after an initial stage of melting and foundered layered intrusions that have sunk out of heated (weakened) crust into the upper mantle (e.g. Glazner, 1994). The more evolved portions of layered intrusions, which contain cumulus ilmenite and apatite, appear to be especially attractive sources for melts similar to TJ, i.e. jotunites or monzonorites.

Isotopic analyses of anorthositic rocks from a given massif typically define mixing arrays between a more evolved crustal component and a more primitive component, whose provenance (enriched mantle, mafic crust) remains unclear. The overall isotopic variations show no consistent correlation with major elements except for a general tendency for troctolitic anorthosites to be more primitive isotopically than noritic anorthosites from the same massif (Ashwal, 1993; Wiebe, 1994). The overall lack of correlation of isotopic and major element variations suggests that the variations were imparted at depth where mantle-derived liquids fractionate away from the compositions characteristic of liquids parental to massif anorthosites, even while assimilating granite. The more isotopically evolved compositions of many noritic anorthosites are consistent with a few percent high-level assimilation of granitic component into a more troctolitic plagioclase suspension. Mantle-derived magmas not only require more granitic component for this transformation than the isotopes allow in many cases, but they are probably blocked by the olivine + augite + plagioclase thermal divide as well.

ACKNOWLEDGEMENTS

We thank D. J. Ellis and R. A. Wiebe for critical reviews that helped us to improve our presentation. We also thank J. H. Berg for providing us with samples from the Hettasch intrusion. Financial support to J. Vander Auwera and J. C. Duchesne was provided by the Belgian Fund for Joint Basic Research and to J. Longhi by NASA Grants NAG-9-329 and NAGW 3407. This work was also part of the International Geological Correlation Programme, Project 290. This paper is Lamont–Doherty Earth Observatory Contribution 5856.

REFERENCES

Agee, C. A. & Walker, D. (1989). Static compression and flotation in ultrabasic silicate liquid. *Journal of Geophysical Research* **93,** 3437–3449.

Andersson, M., Lie, J. E. & Husebye, E. S. (1996). Tectonic setting of post-orogenic granites within SW Fennoscandia based on deep seismic and gravity data. *Terra Nova* **8,** 558–566.

Arndt, N. T. & Goldstein, S. L. (1989). An open boundary layer between lower continental crust and mantle: its role in crust formation and crustal recycling. *Tectonophysics* **161,** 201–212.

Ashwal, L. D. (1993). *Anorthosites*. Berlin: Springer-Verlag, 422 pp.

Ashwal, L. D. & Wooden, J. L. (1983). Isotopic evidence from the eastern Canadian shield for geochemical discontinuity in the Proterozoic mantle. *Nature* **306,** 679–680.

Baker, D. R. & Eggler, D. H. (1987). Compositions of anhydrous melts coexisting with plagioclase, augite and olivine or low-Ca pyroxene from 1 atm to 8 kbar: application to the Aleutian volcanic center of Atka. *American Mineralogist* **72,** 12–28.

Bartels, K. S., Kinzler, R. J. & Grove, T. L. (1991). High pressure phase relations of a near-primary high alumina basalt from Medicine Lake Highland, N. California. *Contributions to Mineralogy and Petrology* **108,** 253–270.

Basaltic Volcanism Study Project (BSVP) (1981). *Basaltic Volcanism on the Terrestrial Planets*. New York: Pergamon, 1286 pp.

Beard, J. S. & Lofgren, G. E. (1991). Dehydration melting and water-saturated melting of basaltic and andesitic greenstones and amphibolites at 1, 3, and 6·9 kbar. *Journal of Petrology* **29,** 365–401.

Bender, J., Langmuir, C., Natland, J. & Batiza, R. (1986). Petrogenesis of East Pacific Rise high-silica glasses. *Eos Transactions, American Geophysical Union* **67,** 1254.

Berg, J. H. (1977). Dry granulite mineral assemblages in the contact aureoles of the Nain Complex, Labrador. *Contributions to Mineralogy and Petrology* **64,** 32–52.

Berg, J. H. (1980). Snowflake troctolite in the Hettasch Intrusion, Labrador: evidence for magma-mixing and supercooling in a plutonic environment. *Contributions to Mineralogy and Petrology* **72,** 339–351.

Bottinga, Y. & Weill, D. F. (1970). Densities of liquid silicate systems calculated from partial molar volumes of oxide components. *American Journal of Science* **287,** 169–182.

Carmichael, I. S. E. (1974). *Igneous Petrology*. New York: McGraw–Hill, 739 pp.

Demaiffe, D. & Hertogen, J. (1981). Rare earth element geochemistry and strontium isotopic composition of a massif-type anorthositic–charnockitic body: the Hidra massif (Rogaland, SW Norway). *Geochimica et Cosmochimica Acta* **45,** 1545–1561.

Demaiffe, D., Weis, D., Michot, J. & Duchesne, J. C. (1986). Isotopic constraints on the genesis of the Rogaland anorthositic suite, southwest Norway. *Chemical Geology* **57,** 167–179.

Demaiffe, D., Bingen, B., Wertz, P. & Hertogen, J. (1990). Geochemistry of the Lyngdal hyperites, S.W. Norway: comparisons with the monzonorites associated with the Rogaland anorthosite complex. *Lithos* **24,** 237–250.

Duchesne, J. C. (1984). Massif anorthosites: another partisan review. In: Brown, W.L. (ed.) *Feldspars and Feldspathoids*. Boston, MA: Reidel, pp. 411–433.

Duchesne, J. C. (1987). The Bjerkreim–Sokndal massif. In: Maijer, C. & Padget, P. (eds) *The Geology of Southernmost Norway: an Excursion Guide. Norges Geologiske Undersøkelse, Special Publication* **1,** 56–59.

Duchesne, J. C. & Demaiffe, D. (1978). Trace elements and anorthosite genesis. *Earth and Planetary Science Letters* **38,** 249–272.

Duchesne, J. C. & Hertogen, J. (1988). Le magma parental du lopolithe de Bjerkreim–Sokndal, Norvège méridionale. *Comptes Rendus de l'Académie des Sciences* **306,** 45–48.

Duchesne, J. C. & Maquil, R. (1987). The Egersund–Ogna massif. In: Maijer, C. & Padget, P. (eds) *The Geology of Southernmost Norway: an Excursion Guide. Norges Geologiske Undersøkelse, Special Publication* **1,** 50–56.

Duchesne, J. C. & Michot, J. (1987). The Rogaland intrusive masses. In: Maijer, C. & Padget, P. (eds) *The Geology of Southernmost Norway: an Excursion Guide. Norges Geologiske Undersøkelse, Special Publication* **1,** 48–50.

Duchesne, J. C., Wilmart, E., Demaiffe, D. & Hertogen, J. (1989). Monzonorites from Rogaland, Southwest Norway: a series of rocks coeval with but not comagmatic with massif-type anorthosites. *Precambrian Research* **7,** 111–128.

Emslie, R. F. (1970). The geology of the Michikamau intrusion, Labrador. *Geological Survey of Canada Paper* **68-57,** 85 pp.

Emslie, R. F. (1975). Pyroxene megacrysts from anorthositic rocks: a new clue to the sources and evolution of the parent magmas. *Canadian Mineralogist* **13,** 138–145.

Emslie, R. F. (1980). Geology and petrology of the Harp Lake Complex, central Labrador: an example of Elsonian magmatism. *Geological Survey of Canada Bulletin* **293,** 1–136.

Emslie, R. F. (1985). Proterozoic anorthosite massifs. In: Tobi, A. C. & Touret, J. L. R. (eds) *The Deep Proterozoic Crust in the North Atlantic Provinces*. Dordrecht: Reidel, pp. 39–60.

Emslie, R. F., Hamilton, M. A. & Therault, R. J. (1994). Petrogenesis of mid-Proterozoic anorthosite–mangerite–charnockite–granite, AMCG complex: isotopic and chemical evidence from the Nain Plutonic Suite. *Journal of Geology* **102,** 539–558.

Fram, M. S. & Longhi, J. (1992). Phase equilibria of dikes associated with Proterozoic anorthosite complexes. *American Mineralogist* **77,** 605–614.

Frost, B. R., Frost, C. D., Lindsley, D. H., Scoates, J. S. & Mitchell, J. N. (1993). The Laramie anorthosite complex and Sherman batholith: geology, evolution and theories of origin. In: Snoke, A. W., Steidtmann, J. R. & Roberts, S. M. (eds) *Geology of Wyoming, Geological Survey of Wyoming Memoir* **5,** 118–161.

Fuhrman, M., Frost, B. R. & Lindsley, D. H. (1988). Crystallization conditions of the Sybille monzosyenite, Laramie Anorthosite Complex, Wyoming. *Journal of Petrology* **29,** 699–729.

Ghiorso, M. S. & Kelemen, P. B. (1987). Evaluating reaction stoichiometry in magmatic systems evolving under generalized thermodynamic constraints: examples comparing isothermal and isenthalpic assimilation. In: Mysen, B. O. (ed.) *Magmatic Processes: Physicochemical Principles. Geochemical Society Special Publication* **1,** 319–336.

Glazner, A. F. (1994). Foundering of mafic plutons and density stratification of continental crust. *Geology* **22,** 435–438.

Green, T. H. (1969). High pressure experimental studies on the origin of anorthosites. *Canadian Journal of Earth Science* **6,** 427–440.

Grove, T. L. & Juster, T. C. (1989). Experimental investigation of low-Ca pyroxene stability and olivine–pyroxene–plagioclase–liquid equilibria at 1-atm in natural basaltic and andesitic liquids. *Contributions to Mineralogy and Petrology* **103,** 287–305.

Hess, H. H. (1960). Stillwater igneous complex, Montana—a quantitative mineralogical study. *Geological Society of America Memoir* **80,** 230 pp.

Jansen, J. B. H., Blok, R. J. P., Bos, A. & Scheelings, M. (1985). Geothermometry and geobarometry in Rogaland and preliminary results from the Bamble area. In: Tobi, A. C. & Touret, J. L. R. (eds.) *The Deep Proterozoic Crust in the North Atlantic Provinces*. Dordrecht: Reidel, pp. 499–516.

Kelemen, P. B. (1990). Reaction between ultramafic rock and fractionating basaltic magma I. Phase relations, the origin of calc-alkaline magma series and the formation of discordant dunite. *Journal of Petrology* **31,** 51–98.

Kinzler, R. J. & Grove, T. L. (1992). Primary magmas of mid-ocean ridge basalts. I: Experiments and methods. *Journal of Geophysical Research* **97,** 6885–6906.

Kolker, A. & Lindsley, D. H. (1989). Geochemical evolution of the Maloin Ranch pluton, Laramie Anorthosite Complex, Wyoming. *American Mineralogist* **74,** 415–446.

Longhi, J. (1987). Liquidus equilibria and solid solution in the system Anorthite–Forsterite–Wollastonite–Silica at low pressure. *American Journal of Science* **287,** 265–331.

Longhi, J. (1991). Comparative liquidus equilibria of hypersthene-normative basalts at low pressure. *American Mineralogist* **76,** 785–800.

Longhi, J. (1992). Origin of green glass magmas by polybaric fractional fusion. *Proceedings of Lunar and Planetary Science 22*. Houston, TX: The Lunar and Planetary Institute, pp. 343–353.

Longhi, J. & Bertka, C. M. (1996). Graphical analysis of pigeonite–augite liquidus equilibria. *American Mineralogist* **81,** 685–695.

Longhi, J., Fram, M. S., Vander Auwera, J. & Monteith, J. (1993). Pressure effects, kinetics and rheology of anorthositic and related magmas. *American Mineralogist* **77,** 605–616.

Maquil, R. & Duchesne, J. C. (1984). Géothermométrie par les pyroxènes et mise en place du massif anorthositique d'Egersund–Ogna (Rogaland, Norvège méridionale). *Annales de la Société Géologique de Belgique* **107,** 27–49.

Menuge, J. F. (1988). The petrogenesis of massif anorthosites: a Nd and Sr isotopic investigation of the Proterozoic of Rogaland/Vest-Agder, SW Norway. *Contributions to Mineralogy and Petrology* **98,** 363–373.

Meyers, R. E. & Emslie, R. F. (1977). The Harp dikes and their relationship to the Helikian record in central Labrador. *Canadian Journal of Earth Science* **14,** 2683–2696.

Mitchell, J. N., Scoates, J. S. & Frost, C. D. (1995). High-Al gabbros in the Laramie anorthosite complex, Wyoming: implications for the composition of melts parental to Proterozoic anorthosites. *Contributions to Mineralogy and Petrology* **119,** 166–180.

Mitchell, J. N., Scoates, J. S., Frost, C. D. & Kolker, A. (1996). The geochemical evolution of anorthosite residual magmas in the Laramie anorthosite complex, Wyoming. *Journal of Petrology* **37,** 637–660.

Morse, S. A. (1979). Kiglapait geochemistry I: systematics, sampling and density. *Journal of Petrology* **20,** 555–590.

Morse, S. A. (1982). A partisan review of Proterozoic anorthosites. *American Mineralogist* **77,** 1087–1100.

Nolan, K. M. & Morse, S. A. (1986). Marginal rocks resembling the estimated bulk composition of the Kiglapait Intrusion. *Geochimica et Cosmochimica Acta* **50,** 2381–2386.

Olson, K. E. & Morse, S. A. (1990). Regional Al–Fe mafic magmas associated with anorthosite-bearing terranes. *Nature* **344,** 760–762.

Owens, B. E., Rockow, M. W. & Dymek, R. F. (1993). Jotunites from the Grenville Province, Quebec: petrological characteristics and implications for massif anorthosite petrogenesis. *Lithos,* **30,** 57–80.

Owens, B. E., Dymek, R. F., Tucker, R. D., Brannon, J. C. & Podosek, F. A. (1994). Age and radiogenic isotopic composition of a late- to post-tectonic anorthosite in the Grenville Province: Labrieville massif, Quebec. *Lithos* **31,** 189–206.

Presnall, D. C., Dixon, J. R., O'Donnell, T. H. & Dixon, S. A. (1979). Generation of mid-ocean ridge tholeiites. *Journal of Petrology* **20,** 3–35.

Ranson, W. A. (1981). Anorthosites of diverse types in the Puttååluk Lake area, Nain complex, Labrador. *Canadian Journal of Earth Science* **18,** 26–41.

Robins, B., Tumyr, O., Tysseland, M. & Garman, L. D. (1997). The Bjerkreim–Sokndal layered intrusion, Rogaland, SW Norway: evidence from marginal rocks for a jotunite parent magma. *Lithos* **39,** 121–133.

Rudnick, R. L. & Fountain, D. M. (1995). Nature and composition of the continental crust: a lower crustal perspective. *Reviews of Geophysics* **33,** 267–309.

Scoates, J. & Frost, C. D. (1996). A strontium and neodymium isotopic investigation of the Laramie anorthosites, Wyoming, USA: implications for magma chamber processes and the evolution of magma conduits in Proterozoic anorthosites. *Geochimica et Cosmochimica Acta* **60,** 95–107.

Simmons, C. & Hanson, G. N. (1978). Geochemistry and origin of massif-type anorthosites. *Contributions to Mineralogy and Petrology* **66,** 119–135.

Springer, W. & Seck, H. A. (1997). Partial fusion of basic granulites at 5 to 15 kbar: implications for the origin of TTG magmas. *Contributions to Mineralogy and Petrology* **127,** 30–45.

Stacey, F. D. (1969). *Physics of the Earth*. New York: John Wiley, 324 pp.

Stebbins, J. F., Carmichael, I. S. E. & Moret, L. K. (1984). Heat capacities and entropies of silicate liquids and glasses. *Contributions to Mineralogy and Petrology* **81,** 1–17.

Taylor, S. R. & McLennan, S. M. (1985). *The Continental Crust: its Composition and Evolution*. London: Blackwell, 312 pp.

Taylor, S. R., Campbell, I. H., McCulloch, M. T. & McLennan, S. M. (1984). A lower crustal origin for massif-type anorthosites. *Nature* **311,** 372–374.

Vander Auwera, J. & Longhi, J. (1994). Experimental study of a jotunite: constraints on the parent magma composition and crystallization conditions, P, T, fO_2 of the Bjerkreim–Sokndal layered intrusion, Norway. *Contributions to Mineralogy and Petrology* **118,** 60–78.

Vander Auwera, J., Longhi, J. & Duchesne, J.-C. (1993). Jotunites from the Rogaland Province, Norway: constraints from experimental data and the partitioning of Sr (plag/melt) and Cr (opx/melt). *Eos Transactions, American Geophysical Union* **74,** 659.

Vander Auwera, J., Longhi, J. & Duchesne, J. C. (1998). A liquid line of descent of the jotunite (hypersthene monzodiorite) suite. *Journal of Petrology* **39,** 439–468.

Walter, M. J. & Presnall, D. C. (1994). Melting behavior of simplified lherzolite in the system CaO–MgO–Al_2O_3–SiO_2–Na_2O from 7 to 35 kbar. *Journal of Petrology* **35,** 329–360.

Wiebe, R. A. (1983). The geologic setting of the Tigalak layered intrusion. In: Morse, S. A. (ed.) *The Nain Anorthosite Project, Labrador: Field Report 1981*. Amherst: University of Massachusetts, pp. 75–78.

Wiebe, R. A. (1985). Proterozoic basalt dikes in the Nain anorthosite complex, Labrador. *Canadian Journal of Earth Sciences* **22,** 1149–1157.

Wiebe, R. A. (1986). Lower crustal cumulate nodules in Proterozoic dikes of the Nain complex: evidence for the origin of Proterozoic anorthosites. *Journal of Petrology* **27,** 1253–1275.

Wiebe, R. A. (1988). Structural and magmatic evolution of a magma chamber: the Newark Island layered intrusion, Nain, Labrador. *Journal of Petrology* **29,** 383–411.

Wiebe, R. A. (1994). Proterozoic anorthosite complexes. In: Condie, K. C. (ed.) *Proterozoic Crustal Evolution*. Amsterdam: Elsevier, pp. 215–261.

Wiebe, R. A. & Snyder, D. (1993). Slow, dense replenishments of a basic magma chamber: the layered series of the Newark Island layered intrusion, Nain, Labrador. *Contributions to Mineralogy and Petrology* **113,** 59–72.

Wilson, J. R., Robins, B. & Duchesne, J. C. (1992). The Bjerkreim–Sokndal intrusion. In: Duchesne, J. C. (ed.) *The Rogaland Intrusive Massifs: an Excursion Guide. International Geological Correlation Programme Project* **290,** 26–39.

Wilson, J. R., Robins, B., Nielsen, F. M., Duchesne, J. C. & Vander Auwera, J. (1996). The Bjerkreim–Sokndal layered intrusion, southwest Norway. In: Cawthorn, R. G. (ed.) *Layered Intrusions*. Amsterdam: Elsevier, pp. 231–255.

Xue, S. & Morse, S. A. (1993). Geochemistry of the Nain massif anorthosite: magma diversity in five intrusions. *Geochimica et Cosmochimica Acta* **57,** 3925–3948.